Identifying and correcting interferences to PTR-ToF-MS measurements of isoprene and other urban volatile organic compounds

Matthew M. Coggon[1*], Chelsea E. Stockwell[1,2], Megan S. Claflin[3], Eva Y. Pfannerstill[4], Xu Lu[1,2], Jessica B. Gilman[1], Julia Marcantonio[5], Cong Cao[5], Kelvin Bates[1,2], Georgios I. Gkatzelis[6], Aaron Lamplugh[7], Erin F. Katz[4,8], Caleb Arata[4], Eric C. Apel[9], Rebecca S. Hornbook[9], Felix Piel[10,11,12], Francesca Majluf[3,a], Donald R. Blake[13], Armin Wisthaler[10,11] Manjula Canagaratna[3], Brian M. Lerner[3], Allen H. Goldstein[4,14], John E. Mak[5], Carsten Warneke[1]

[1]NOAA Chemical Sciences Laboratory, Boulder, CO, 80305, USA
[2]Cooperative Institute for Research in Environmental Sciences, University of Colorado, Boulder, CO, 80305, USA
[3]Aerodyne Research, Inc., Billerica, MA, 01821, USA
[4]Department of Environmental Science, Policy, & Management, University of California Berkeley, Berkeley, CA, 94720, USA
[5]School of Marine and Atmospheric Science, Stony Brook University, Stony Brook, NY 11794, USA
[6]IEK-8: Troposphere, Forschungszentrum Jülich GmbH, Jülich, Germany
[7]Institute of Behavioral Science, University of Colorado, Boulder, CO, 80305, USA
[8]Department of Chemistry, University of California Berkeley, Berkeley, CA, 94720, USA
[9]Atmospheric Chemistry Observations & Modeling Laboratory, NCAR, Boulder, CO, 80301, USA
[10]Department of Chemistry, University of Oslo, Oslo, Norway
[11]Institut für Ionenphysik und Angewandte Physik, Universität Innsbruck, Innsbruck, Austria
[12]IONICON Analytik GmbH, Innsbruck, Austria
[13]Department of Chemistry, University of California, Irvine, CA, 92697, USA
[14]Department of Civil and Environmental Engineering, University of California Berkeley, Berkeley, CA, 94720, USA
[a.]Now at Olin College of Engineering, Needham, MA, 02492

*Corresponding author: matthew.m.coggon@noaa.gov

Abstract: Proton-transfer-reaction time-of-flight mass spectrometry (PTR-ToF-MS) is a technique commonly used to measure ambient volatile organic compounds (VOCs) in urban, rural, and remote environments. PTR-ToF-MS is known to produce artifacts from ion fragmentation, which complicates the interpretation and quantification of key atmospheric VOCs. This study evaluates the extent to which fragmentation and other ionization processes impacts urban measurements of the PTR-ToF-MS ions typically assigned to isoprene (m/z 69, $C_5H_8H^+$), acetaldehyde (m/z 45, CH_3CHO^+), and benzene (m/z 79, $C_6H_6H^+$). Interferences from fragmentation are identified using gas-chromatography (GC) pre-separation and the impact of these interferences are quantified using ground-based and airborne measurements in a number of

44 US cities, including Las Vegas, Los Angeles, New York City, and Detroit. In urban regions with
45 low biogenic isoprene emissions (e.g., Las Vegas), fragmentation from higher carbon aldehydes
46 and cycloalkanes emitted from anthropogenic sources may contribute to m/z 69 by as much as
47 50% during the day, while the majority of the signal at m/z 69 is attributed to fragmentation during
48 the night. Interferences are a higher fraction of m/z 69 during airborne studies, which likely results
49 from differences in the reactivity between isoprene and the interfering species along with the
50 subsequent changes to the VOC mixture at higher altitudes. For other PTR masses, including m/z
51 45 and m/z 79, interferences are observed due to the fragmentation and secondary ionization of
52 VOCs typically used in solvents, which are becoming a more important source of anthropogenic
53 VOCs in urban areas. We present methods to correct these interferences, which provide better
54 agreement with GC measurements of isomer specific molecules. These observations show the
55 utility of deploying GC pre-separation for the interpretation PTR-ToF-MS spectra.
56
57 **1. Introduction**
58
59 Volatile organic compounds (VOCs) are an important contributor to urban air pollution. Once
60 emitted to the atmosphere, VOCs undergo chemical reactions that contribute to the formation of
61 hazardous pollutants such as ozone and secondary organic aerosol. It is important to quantify VOC
62 mixing ratios in urban areas to determine strategies that may reduce air pollution.
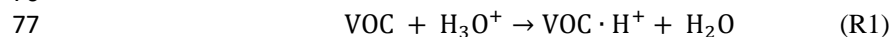63
64 Proton-transfer-reaction time-of-flight mass spectrometry (PTR-ToF-MS) is a technique used to
65 measure a wide spectrum of VOCs, including oxygenates, aromatics, furanoids, nitriles, and
66 biogenic species such as isoprene and monoterpene isomers (Yuan et al., 2017). PTR-ToF-MS
67 measurements in urban regions enable the determination of VOC mixing ratios from an extensive
68 range of emission sources, including fossil fuels, solvent evaporation from volatile chemical
69 products (VCPs), residential wood burning, cooking, and urban foliage (Yuan et al., 2017). The
70 fast-time resolution and broad selectivity of PTR-ToF-MS measurements enables source
71 apportionment, flux estimates, and spatial mapping on mobile platforms that yield important
72 information about urban VOC source strengths (e.g., Gkatzelis et al., 2021a;Karl et al.,
73 2018;Pfannerstill et al., 2023)
74
75 VOC detection by PTR-ToF-MS relies on analyte reactions with protonated water (Reaction 1).
76
77 $$\mathrm{VOC\ +\ H_3O^+ \rightarrow VOC \cdot H^+ +\ H_2O} \qquad \text{(R1)}$$
78
79 Proton transfer is exothermic and spontaneous for VOCs with a proton affinity that is greater than
80 water. For many VOCs, including ketones, aromatics, and nitriles, the protonated product
81 $(\mathrm{VOC \cdot H^+})$ is the primary signal detected by PTR-ToF-MS. For other VOCs, secondary reactions
82 including dehydration, fragmentation, and water clustering results in additional product ions that
83 can complicate the mass spectra. Pagonis et al. (2019) summarizes studies that have reported
84 fragmentation for a wide spectrum of species. Fragmentation is most prevalent in alcohols,
85 aldehydes, and other species with long-chain alkane functionality. Small alcohols and aldehydes
86 $(\mathrm{C} < 3)$ primarily react to form protonated products following R1, while at higher carbon numbers,
87 a large fraction of the reactions follow dehydration and/or fragmentation (R2-R3).
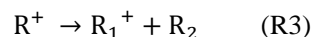88
89 $$\mathrm{(R - OH, RH = O) \cdot H^+ \rightarrow R^+ +\ H_2O} \qquad \text{(R2)}$$

90

91 $$R^+ \rightarrow R_1^+ + R_2 \qquad \text{(R3)}$$

92

93 R is the carbon backbone of an alcohol (R-OH) or aldehyde (RH=O), R^+ is the dehydration product,
94 R_1^+ is a fragment, and R_2 is a neutral product. Fragmentation may also result from protonation of
95 cycloalkanes or alkyl aromatics. PTR-ToF-MS is not sensitive to small alkanes (C < 5), but larger
96 alkanes and cycloalkanes are detected at low sensitivity and upon ionization subsequently
97 fragment to produce ions that often overlap with the dehydration and fragmentation products of
98 alcohols and aldehydes (Arnold et al., 1998;Gueneron et al., 2015;Jobson et al., 2005). The degree
99 of dehydration and fragmentation is partially dependent on the strength of the drift field (E) and
100 density (N) (characterized by the E/N ratio), which impacts ion kinetic energy (Arnold et al.,
101 1998;Krechmer et al., 2018;Yuan et al., 2017;Holzinger et al., 2019). Lower E/N results in lower
102 fragmentation, but higher clustering with neutral water, which may further complicate the mass
103 spectra (Holzinger et al., 2019). Additional products may also be formed by reactions of analytes
104 with O_2^+ and NO^+ ions, which are present due to the ionization of small amounts of air in the
105 discharge region.

106

107 In the atmosphere, complex mixtures of emissions may result in PTR-ToF-MS mass spectra where
108 dehydration and fragmentation products interfere with the quantification of important atmospheric
109 VOCs. For example, PTR-ToF-MS measurements in regions with significant oil and natural gas
110 development show that substituted cycloalkanes fragment to produce significant signal at m/z 69
111 ($C_5H_9^+$, Koss et al., 2017;Warneke et al., 2014;Pfannerstill et al., 2019). Likewise, interferences
112 have been observed downwind of urban and industrial environments (e.g., Inomata et al.,
113 2010;Choi et al., 2022). These fragments overlap with protonated isoprene and these previous
114 studies have shown that interferences make isoprene quantification challenging in these regions.
115 In forested areas, isoprene is largely emitted from biogenic sources and previous studies that have
116 compared PTR-ToF-MS measurements to those from gas-chromatography show good agreement
117 (e.g., Kaser et al., 2013). The impact of an interference to specific molecules, such as isoprene,
118 depends on atmospheric composition which changes spatially (e.g., urban vs. rural regions) and
119 temporally (e.g., summer vs. winter).

120

121 Assessments of interferences on PTR-MS measurements in urban atmospheres have been
122 conducted previously (e.g., Warneke et al., 2003), but the sources that contribute to urban VOCs
123 change on decadal timescales as fossil fuel emissions steadily decline (Kim et al., 2022;Warneke
124 et al., 2012). The urban atmospheric composition, once dominated by motor vehicle emissions, is
125 now composed of a higher proportion of oxygenates from solvents, other VOCs emitted from
126 sources such as VCPs, and cooking (Gkatzelis et al., 2021b;McDonald et al., 2018;Peng et al.,
127 2022;Wernis et al., 2022). Significant advances in PTR-ToF-MS detectors (quadrupole vs time-
128 of-flight mass spectrometers) and drift tube designs have enhanced instrument capabilities to
129 acquire mass spectra with greater resolution and sensitivity (Breitenlechner et al., 2017;Krechmer
130 et al., 2018;Yuan et al., 2016;Holzinger et al., 2019). These technological advances enable better
131 identification and quantification and also an improved understanding of the interferences that
132 impact PTR-ToF-MS spectra.

133

134 With the changes in atmospheric composition and technological advances, it is necessary to revisit
135 potential interferences to commonly observed and reported VOCs by PTR-ToF-MS. In this study,

136 we investigate the interferences that impact PTR-ToF-MS spectra measured across several US
137 urban areas including Los Angeles, CA, Las Vegas, NV, Detroit, MI, and New York City, NY.
138 Interferences are identified using GC pre-separation, similar to previous measurements that
139 quantified PTR-ToF-MS fragmentation and interferences observed in complex mixtures, including
140 wildfire and urban emissions (e.g., Koss et al., 2018;Warneke et al., 2003). We show that
141 commonly measured species, such as acetaldehyde, benzene, and isoprene, exhibit interferences
142 from larger molecules associated with solvent use and cooking. The extent of these interferences
143 depends on the temporal and spatial variability of VOC emission sources. We present methods to
144 correct for these interferences based on the measurement capabilities of modern PTR-ToF-MS
145 instruments.
146
147 **2. Methods**
148
149 Table 1 summarizes the key field campaigns and instrumentation used to quantify VOCs and PTR-
150 ToF-MS interferences. Multiple PTR-ToF-MS instruments are used in this study and Table 1
151 outlines the PTR-ToF-MS reactor designs and drift tube operating parameters that play an
152 important role in determining ion distributions. In this study, all instruments were operated with
153 E/N 120 – 140 Td. The instruments described in this study use ion-molecular reactors and ion
154 optics devolved by Ionicon Analytik and Tofwerk, AG as described by Müller et al. (2014) and
155 Krechmer et al. (2018), respectively. The following sections describe each campaign and provide
156 additional details of instrument operation
157
158 **Table 1:** Summary of campaigns, instrumentation, drift tube operating parameters, and interferences reported for each
159 campaign.

Campaign	Location	Dates	Instrumentation	Reactor Design[1]	E/N (Td)	Studied Interferences
SUNVEx	Las Vegas, NV	July 1 – 30, 2021	NOAA PTR-ToF-MS[2] NOAA GC-PTR-ToF-MS NOAA iWAS	Vocus	140	Isoprene, aromatics, oxygenates
RECAP-CA	Los Angeles, CA; Central Valley, CA	June 1 – Aug 30, 2021	NOAA PTR-ToF-MS[2] UC Berkeley PTR-ToF-MS[2] NOAA GC-MS	Vocus (NOAA) Vocus (Berkeley)	140 130	Isoprene, aromatics, oxygenates
FIREX-AQ	Los Angeles, CA	September 5, 2019	NOAA PTR-ToF-MS[2] Oslo PTR-ToF-MS[3] NOAA iWAS, UCI Irvine WAS NCAR TOGA-TOF	HC / DT (NOAA) HC/ DT (Oslo)	125 120	Isoprene
MOOSE	Detroit, MI	May 21 – June 30, 2021	Aerodyne PTR-ToF-MS[2] Aerodyne GC-EI-ToF-MS	Vocus	125	Isoprene, aromatics
LISTOS	New York City, NY	January 2020 – April 2021.	Stony Brook PTR-ToF-MS[3]	HC / DT	130	Isoprene

160
161 [1] HC / DT refers to the hollow cathode / drift tube design used in traditional PTR-MS instruments. This reactor is used in this study with both
162 Tofwerk and Ionicon systems. The Vocus reactor is used with Tofwerk instruments.
163 [2] Tofwerk design PTR-ToF-MS using quadrupole ion optics as described by Krechmer et al. (2018)
164 [3] Ionicon design PTR-ToF-MS with ion optics consisting of two einzel lens as described by Müller et al. (2014)
165
166 **2.1.Campaign Descriptions**
167
168 **2.1.1. SUNVEx / RECAP-CA**
169
170 PTR-ToF-MS measurements were performed as part of the 2021 Southwest NO$_x$ and VOC
171 Experiment (SUNVEx, https://csl.noaa.gov/projects/sunvex/) and Re-Evaluating the Chemistry of

172 Air Pollutants in California (RECAP-CA). SUNVEx was a ground campaign conducted to study
173 air quality in the Las Vegas Valley during the summer ozone season using both mobile and ground-
174 based sampling. The RECAP-CA campaign was conducted in Los Angeles and included mobile,
175 ground-based, and airborne sampling.
176
177 Measurements in Las Vegas were conducted between 30 June–27 July 2021 at an air quality
178 monitoring station located near the Jerome Mack Middle School (Fig. 1). Jerome Mack is an urban
179 background site located ~ 8km east of downtown Las Vegas. The site was chosen based on its
180 suite of trace gas and $PM_{2.5}$ monitors and classification as a US Environmental Protection Agency
181 (EPA) Photochemical Assessment Monitoring Station (Annual Monitoring Network Plan, 2022).

182 Measurements in the Los Angeles Basin were conducted between 2 August and 5 September 2021
183 at the California Institute of Technology in Pasadena, CA (Caltech, Fig. 1). The ground site was
184 located within 0.5 km of the site used during the California Research at the Nexus of Air Quality
185 and Climate Change (CalNex) field study in order to directly compare with air quality
186 measurements conducted in 2010 (Ryerson et al., 2013). During this portion of the campaign,
187 instruments were situated in a trailer and sampled air from the top of a 10-m tower.

188 During both SUNVEx and RECAP-CA, the NOAA mobile laboratory was deployed to sample the
189 spatial distribution of VOCs and NO_x in regions of varying population density. A similar sampling
190 strategy was employed previously to study urban VOC enhancements in New York City and is
191 useful for identifying VOC signatures emitted from major sources, such as fossil fuels, VCPs, and
192 cooking activities (Coggon et al., 2021;Gkatzelis et al., 2021a;Gkatzelis et al., 2021b;Stockwell et
193 al., 2021). Drive tracks from the mobile laboratory are shown on the map in Fig. 1, along with the
194 locations of the ground sites and major population centers.
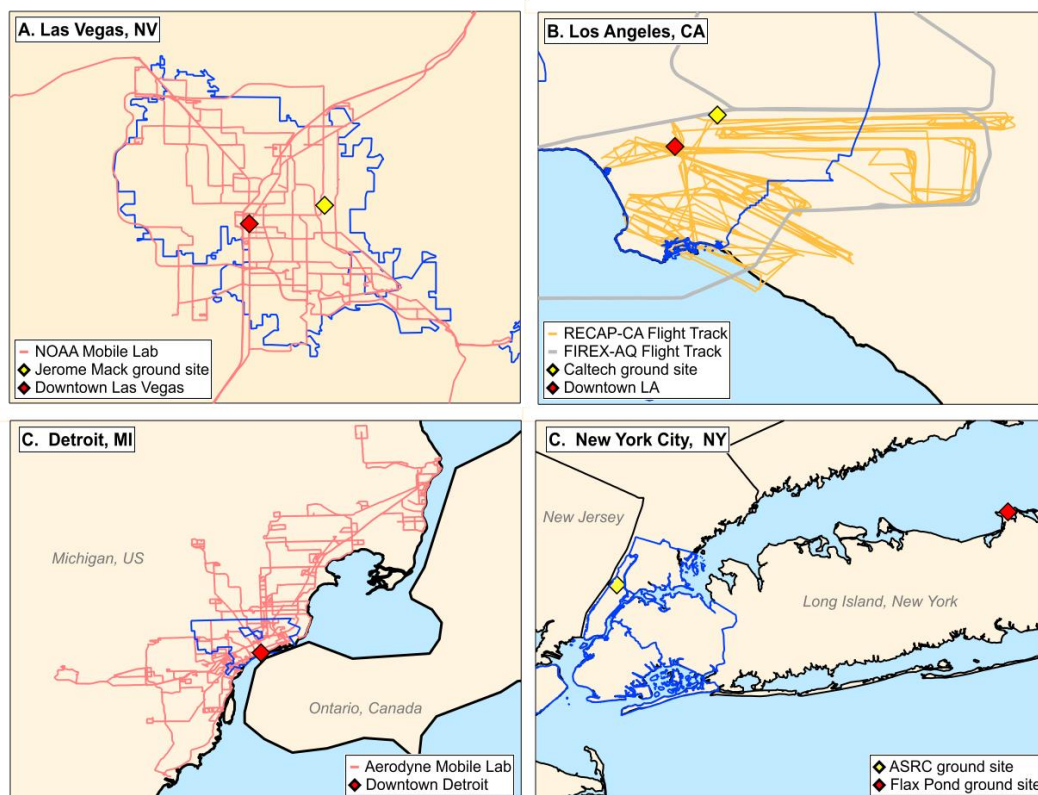
Figure 1. Mobile laboratory drive tracks, flight tracks, ground site locations, and locations of interest for the field campaigns outlined in Table 1. The blue lines highlight the statistical metropolitan areas for Las Vegas, Los Angeles, and Detroit, and the five boroughs of New York City.

The airborne component of RECAP-CA was conducted onboard the Naval Postgraduate School UV-18A Twin Otter aircraft and was based out of an airport located in Burbank, CA. Measurements of VOCs, NO_x, and greenhouse gases took place on nine days between 1 June and 23 June 2021. The Twin Otter typically flew at ~ 300 m above ground level at air speeds of 50 – 60 m s^{-1}. Each flight covered approximately 5000 km of distance across the Los Angeles area, including downtown, the coast, the Santa Ana area, and the San Bernardino Valley. The flight track of the Twin Otter is shown in Fig. 1b.

2.1.2. FIREX-AQ

The 2019 Fire Influence on Regional to Global Environments and Air Quality (FIREX-AQ) campaign was a large field study designed to investigate the emissions and atmospheric chemistry of biomass burning emissions. A detailed description of the campaign, instrumentation, and science goals is provided by Warneke et al. (2023). As part of the measurements, urban flights were performed through the Los Angeles Basin on 5 September 2019. VOC measurements were conducted onboard the NASA DC-8 by the NOAA PTR-ToF-MS and University of Oslo PTR-

215 ToF-MS. VOC measurements were also conducted by three GC instruments: the NOAA improved
216 Whole Air Sampler (iWAS), the University of California, Irvine Whole Air Sampler (WAS) and
217 the NCAR Trace Organic Gas Analyzer with a Time-of-Flight mass spectrometer (TOGA-TOF).
218 The flight tracks conducted in Los Angeles are shown in Fig. 1b.
219
220 **2.1.3. MOOSE Campaign**
221
222 The Michigan-Ontario Ozone Source Experiment (MOOSE) campaign was a multi-institutional
223 ground-based and mobile sampling effort conducted in 2021 to study ozone, meteorology, and
224 pollution in and around Michigan and Ontario. This region is currently designated as non-
225 attainment of the US federal ozone standard. Aerodyne Research, Inc. scientists deployed the
226 Aerodyne Mobile Laboratory (Herndon et al., 2005;Yacovitch et al., 2015) as part of the
227 CHEmical Source Signatures (CHESS) sub-experiment in order to measure emission plumes from
228 point sources and gain insight to the drivers of local ozone pollution during MOOSE. Other goals
229 of CHESS included developing emission source fingerprints for significant industrial source sites
230 in the area.
231
232 Ambient VOC measurements were conducted onboard the mobile laboratory using a PTR-TOF-
233 MS which was co-located with an *in situ* GC-EI-TOF-MS equipped with thermal desorption
234 preconcentration (Claflin et al., 2021). The AML sampled air around the Detroit metropolitan
235 region between 21 May and 30 June 2021 (Fig 1c). During mobile sampling, the mobile laboratory
236 transited through major population centers and targeted industrial point sources. Overnight and
237 when not driving, the mobile laboratory was stationed at the Salina Elementary/Intermediate
238 Schools in Dearborn, MI, parked at the Michigan Department of Environment, Great Lakes, and
239 Energy air monitoring station [AQS ID 26-163-0033].
240
241 **2.1.4. LISTOS**
242
243 The Stony Brook PTR-ToF-MS was deployed on the rooftop observatory at the Advanced
244 Sciences Research Center (ASRC) of the City University of New York to make continuous, high
245 time-resolution measurements of VOCs during the COVID lockdown from January 2020 to April
246 2021, (Fig. 1c; Cao et al., 2023). This campaign was a part of the broader Long Island Sound
247 Tropospheric Ozone Study (LISTOS). ASRC is located in the Manhattan Borough of New York
248 City, which is a highly urbanized region. Air was continuously sampled from a rooftop observatory
249 that is situated ~90 m above sea level on one of the tallest buildings in the vicinity of the site. In
250 June 2022, the Stonybrook PTR-ToF-MS was moved to the Flax Pond Marine Laboratory
251 (40°57′36″N, 73°8′24″ W) near Stony Brook, New York, which is about 60 miles east of ASRC
252 and located on the north side of Long Island in a forested suburban area. The Flax Pond Marine
253 Laboratory is a 0.6 km^2 preserve that encompasses a tidal wetland area and is operated for research
254 purposes by the School of Marine and Atmospheric Sciences of Stony Brook University. At Flax
255 Pond, air was continuously sampled from a ~10 m tower.
256
257 **2.2.Instrument Descriptions – PTR-ToF-MS**
258
259 **2.2.1. NOAA PTR-ToF-MS**
260

261 The NOAA PTR-ToF-MS was deployed during SUNVEx, RECAP-CA, and FIREX-AQ. During
262 FIREX-AQ, the NOAA PTR-ToF-MS used a traditional ion source and drift tube as described by
263 Yuan et al. (2016). A full description of the operating parameters, VOC measurements, and
264 calibration methods are provided by Gkatzelis et al. (2022).

266 During SUNVEx and RECAP-CA, the instrument was modified to use the Vocus focusing ion
267 molecule reactor (TOFWERK, AG) and was operated following the recommendations by
268 Krechmer et al. (2018). The Vocus provides greater sensitivity to VOCs compared to the
269 traditional drift tube design due to the use of quadrupole ion guides that increase ion transmission.
270 Here, the Vocus was operated at 2.5 mbar and with an axial electric field gradient of 65 V cm^{-1}
271 (E/N ~ 140 Td). The water flow to the ion source was maintained at 23 mL min^{-1} and the drift tube
272 was heated to 110°C. Typically, the quadrupole ion guide in the Vocus PTR-ToF-MS is operated
273 at voltages > 275 V to reduce the transmission of reagent ions that would otherwise limit the
274 lifetime of the detectors (Krechmer et al., 2018). Here, the quadrupole ion guide was tuned to 250
275 V to increase the transmission of ions produced from important VOCs with low molecular weights,
276 such as ethanol (m/z 47), acetonitrile (m/z 42), and methanol (m/z 33). Figure S1 compares the
277 product distribution of VOCs measured by the Vocus against those measured with the traditional
278 drift tube. In general, the ion product distributions are comparable, though small differences in
279 water clusters and fragmentation in the Vocus reflect the higher amount of water in the drift tube
280 and a higher operating E/N. The degree of fragmentation in the NOAA Vocus PTR-ToF-MS is
281 comparable to other PTR-MS systems with E/N > 120 Td (e.g., Buhr et al., 2002; Pagonis et al.,
282 2019). Other Vocus PTR-ToF-MS instruments used in this study observed higher fragmentation
283 owing to differences in operating conditions of the big-segmented quadrupole (BSQ). The
284 implications of fragmentation from the BSQ are discussed further in Section 3.1.

286 To guide the identification of the proton-transfer-reaction products, a GC was used to trap and pre-
287 separate ambient VOCs during SUNVEx. The GC deployed here is the same instrument used by
288 Stockwell et al. (2021) to identify molecular isomers measured from coating headspaces. Briefly,
289 the GC consists of a liquid nitrogen cryotrap coupled to a DB-624 column (Restek MXT-624; 30-
290 m length × 0.25-mm inner diameter (I.D.), 1.4-μm film thickness). Samples were collected onto
291 the cryotrap at predetermined volumes (typically 80 cm^3), then injected onto the column via rapid
292 heating to 100°C. Nitrogen gas carried the sample through the column at 8 sccm while the column
293 was heated from 40°C to 150°C at a rate of 12°C min^{-1}. The effluent from the column was injected
294 into the PTR-ToF-MS inlet. In this study, we use this setup (termed GC-PTR-ToF-MS) to
295 qualitatively assess isomer distributions and fragmentation patterns for VOCs detected during *in*
296 *situ* sampling.

298 The GC-PTR-ToF-MS was primarily deployed during the ground-based sampling phase in Las
299 Vegas, while PTR-ToF-MS only was used in Los Angeles. In GC-mode, samples were collected
300 every 2 hours and automatically analyzed by PTR-ToF-MS. In between GC measurements, the
301 PTR-ToF-MS sampled ambient air through a 10-m Teflon inlet at 2 L min^{-1}. During ambient
302 sampling, instrument backgrounds were determined hourly by passing ambient air through
303 platinum catalyst heated to 350°C. The PTR-ToF-MS was calibrated using gravimetrically-
304 prepared gas standards, or by liquid calibration (Coggon et al., 2018).

306 When installed on the mobile laboratory, the PTR-ToF-MS sampled air through a 1-m Teflon inlet
307 at 2 L min^{-1}, and instrument backgrounds were determined every 15 minutes. During an evening
308 drive on 31 July 2021, the GC-PTR-ToF-MS was deployed to speciate VOCs on the Las Vegas
309 Strip, where large crowds of people were present and anthropogenic emissions from personal care
310 products, cooking, and other human activities were expected to be highest.

311

312 **2.2.2. University of Oslo PTR-ToF-MS**

313

314 The University of Oslo PTR-ToF-MS was deployed during FIREX-AQ to target NH_3, but also
315 measured the same VOCs as the NOAA PTR-ToF-MS. The instrument was operated as described
316 by Müller et al. (2014) with modifications to reduce the formation of NH_4^+ in the ion source as
317 described by Tomsche et al. (2023). Briefly, the instrument sampled air through a heated inlet at a
318 flowrate of 10–60 L min^{-1} in order to reduce losses of NH_3 to inlet surfaces. The drift tube was
319 operated at 2.1 mbar and 120°C with corresponding E/N ratio of 120 Td. VOC sensitivities were
320 determined via calibrated using gravimetrically-prepared standards.

321

322 **2.2.3. University of California Berkeley PTR-ToF-MS**

323

324 The Berkeley Vocus PTR-ToF-MS (Aerodyne Research, Inc., Billerica, USA) was deployed
325 during the RECAP-CA aircraft campaign on the US Navy Twin Otter. The PTR-ToF-MS was
326 operated with a Vocus reactor set to 60°C, 2.0 mbar, and an E/N ratio of ~ 130 Td. The potential
327 gradient along the drift tube was 590 V. The gradient between BSQ skimmer 1 and skimmer 2 was
328 changed once during the campaign from 6 to 9.1 V, which resulted in an improved sensitivity for
329 some VOCs, but significantly stronger fragmentation for other compounds such as nonanal (Fig.
330 S2). Both operating conditions were calibrated. The reagent water flow was 20 mL min^{-1}. Similar
331 to the NOAA-PTR-ToF-MS, the voltage of the quadrupole ion guide was operated at 200 V to
332 improve the transmission for low-mass VOCs like methanol.

333

334 Ambient air was sampled via a 90 cm long heated (40°C) ¼-inch Teflon line through a Teflon
335 filter from an isokinetic inlet (flow rate ~ 6 m s^{-1} for 5 m length) with a mass flow controller at 1.5
336 L min^{-1}. Mass spectra were recorded at 10 Hz time resolution for a mass range of 10-500 Da. Zero-
337 air blank measurements were conducted several times in each flight for 1-5 minutes during aircraft
338 turns ~ 2-4 times per flight, each followed by a pulse of calibration gas ~ 1-5 minutes in duration.
339 These in-flight calibrations were used to validate the sensitivities calculated from ground
340 calibrations. Ground calibrations were conducted every 1-3 days (in total, 19 times) during the
341 campaign using one of three gravimetrically prepared multicomponent VOC standards (Apel-
342 Riemer Environmental Inc., Miami, FL, USA). More details on the instrument operation and
343 calibration can be found in Pfannerstill et al. (2023).

344

345 **2.2.4. Aerodyne PTR-ToF-MS**

346

347 Aerodyne Research, Inc. deployed a Vocus PTR-ToF-MS during MOOSE 2021 (Krechmer et al.,
348 2018;Riva et al., 2019). The Vocus was operated at a pressure of 2.2 mbar and axial voltage
349 gradient of 600 V, corresponding to an E/N ratio of 125 Td. Data were recorded and processed at
350 1 Hz time resolution using the Tofware software (Aerodyne Research Inc. and TOFWERK) in
351 Igor Pro (WaveMetrics) (Stark et al., 2015). Background measurements were conducted every 16

352 minutes by overflowing the Vocus inlet with air from a zero-air generator (ZAG) equipped with a
353 Pt/Pd catalyst at 400°C. Calibrations were performed every 4 hours with a multicomponent VOC
354 mixture (Apel-Riemer Environmental Inc., Miami, FL, USA; nominal 1 ppm in N_2) diluted with
355 ZAG air. The sensitivities of species in the calibration mixture were correlated to their proton-
356 capture-rate coefficient (Sekimoto et al., 2017). To calculate sensitivities for compounds not
357 present in the calibration mixture, the slope of the linear fit was multiplied by the proton-capture-
358 rate coefficient of the species of interest (Holzinger et al., 2019;Krechmer et al., 2018).

359
360 **2.2.5. Stony Brook PTR-ToF-MS**

361
362 The Stony Brook Ionicon high-resolution PTR-ToF-MS (Ionicon 8000, Analytik GmbH, Austria)
363 was deployed in New York City during the COVID shutdown, and subsequently at Flax Pond on
364 Long Island. In this study, the Stony Brook PTR-ToF-MS was operated with a drift field of ~130
365 Td, drift voltage of 600 V, reactor temperature of 60°C, and drift tube pressure of 2.3 mbar. The
366 instrument sampled VOCs through a heated (60°C) 1/16-inch outer diameter (O.D.) capillary
367 PEEK inlet (~1 m length) with bypass flow line teed off the 1/2-inch PTFE inlet line fitted with a
368 blower on the back end (residence time of the gas was ~10 s). Data were collected at 1 Hz and
369 integrated to 5-minute averages.

370 Calibrations were performed using a dynamic dilution system. VOC-free air was produced by
371 pumping ambient air through a Pt-based catalytic converter at 400°C, then mixed with
372 multicomponent gas calibration mixture (Apel-Riemer Environmental Inc., Miami, FL, USA) that
373 included isoprene. Calibration was performed spanning a concentration range of observed values
374 (0, 5, 10, 15, 20 ppbv). At ASRC, the calibration gas was typically analyzed twice a week prior to
375 the COVID-19 lockdown, and typically every 1-2 weeks during the lockdown given limited access
376 to the observatory. At Flax Pond, the calibration gas was analyzed once a week.

377
378 **2.3.Instrument Descriptions – Gas Chromatography**

379
380 **2.3.1. NOAA GC-MS**

381
382 The NOAA GC-MS provided speciated VOC measurements during SUNVEx, RECAP-CA, and
383 FIREX-AQ. During RECAP-CA, the NOAA GC-MS was deployed to the ground site to sample
384 ambient air on a 20 minute duty cycle. The GC-MS collects two separate 240 mL samples and
385 analyzes each on two channels. Channel 1 consists of a CO_2 trap (Ascarite II, Thomas Scientific),
386 a water trap operated at -55°C, and a sample trap operated at -165°C. The series of traps are linked
387 to an Al_2O_3-KCl porous layer open tubular column (Restek RT-Alumina bonded porous
388 polymer/KCl; 30-m length × 0.25-mm I.D., and 4-µm film thickness) designed to separate light
389 hydrocarbons. Channel 2 consists of the water and sample traps, but is coupled to a DB-624 column
390 identical to the column used in the GC-PTR-ToF-MS. This column separates hydrocarbons up to
391 C_{12}, as well as select oxygen-, halogen-, and nitrogen-containing VOCs. The effluent of each
392 column is analyzed using a quadrupole mass spectrometer (Agilent 5975C) operated in selected
393 ion monitoring/scan mode. The GC-MS was calibrated using a gravimetrically-prepared gas
394 mixture containing 50 VOC components.

395
396 VOCs analyzed by NOAA GC-MS in Las Vegas and during FIREX-AQ were first sampled using
397 a whole air sampling canister system (iWAS, Lerner et al., 2017). The iWAS system consists of a

398 stainless steel compressor and 24 2.7 L electropolished stainless steel canisters. During SUNVEx,
399 canisters were filled every 2 hours during stationary ground-based sampling, while targeted
400 samples were taken during mobile drives. During FIREX-AQ, targeted samples were filled on
401 demand up to a total number of 72 per flight. The canisters were shipped to either Boulder, CO, or
402 Pasadena, CA, and analyzed by GC-MS within four days of collection to minimize sampling
403 artifacts.
404
405
406 ### 2.3.2.   UCI WAS
407
408 The University of California, Irvine Whole Air Sampler (UCI WAS) was deployed on the DC-8
409 during FIREX-AQ to sample VOCs and halocarbons. The UCI WAS operated similarly to the
410 NOAA canister system, where samples were collected into electropolished stainless steel canisters,
411 then analyzed offline within seven days using a series of laboratory GC systems. The operation of
412 the airborne WAS and laboratory GCs is fully described elsewhere (Colman et al., 2001;Simpson
413 et al., 2020;Simpson et al., 2010). All samples were analyzed on a multi-column GC system
414 coupled to flame ionization, electron capture, and mass selective detectors. The whole system is
415 calibrated using a suite of VOC standards.
416
417 ### 2.3.3.   TOGA-TOF
418
419 The NCAR Total Organic Gas Analyzer with a TOFWERK electron ionization high-resolution
420 time-of-flight mass spectrometer (TOGA-TOF) was deployed on the DC-8 during FIREX-AQ to
421 provide *in situ* GC measurements of a large suite of VOCs including hydrocarbons, oxygenated
422 VOCs (OVOCs), and halogen-, nitrogen- and sulfur-containing VOCs. A full description of the
423 TOGA system is provided by Apel et al. (2015). Briefly, during FIREX-AQ the TOGA-TOF
424 continuously sampled 13-mL aliquots of ambient air for approximately 35 seconds every 105
425 seconds, concentrating the VOCs in two cryogenic preconcentration steps prior to injection onto a
426 Restek MTX-624 column (I.D. = 0.18 μm, length = 8 m). Helium gas carried the samples through
427 the column, which was heated from 25–120°C at a rate of 100°C min^{-1}, and the effluent was
428 analyzed by the electron ionization time-of-flight mass spectrometer. The TOF-MS was operated
429 at 70 eV and nominal mass resolution 3000 Δm m^{-1}. The system was calibrated several times per
430 flight and in the laboratory before and after the campaign using a series of multicomponent VOC
431 standards (Apel-Riemer Environmental Inc., Miami, FL, USA).
432
433
434 ### 2.3.4.   Aerodyne GC-MS
435
436 The ARI GC-MS system consists of three main components: (1) a thermal desorption
437 preconcentrator (TDPC) (Aerodyne Research, Inc.) for sample collection, (2) a GC (Aerodyne
438 Research, Inc.) for sample separation, and (3) an electron ionization time-of-flight mass
439 spectrometer (EI-ToF-MS) (TOFWERK AG, model EI-HTOF) for sample detection (Gilman et
440 al., 2013; Obersteiner et al., 2016; Claflin et al., 2021). For the MOOSE campaign, the TOF-MS
441 was operated at 70 eV and nominal mass resolution 3000 Δm m^{-1}. The GC is a 2-channel system,
442 where both separation channels use identical preconcentration steps. The TDPC employed for this
443 campaign relied upon two-stage adsorbent trapping for preconcentration of analytes. The sample

444   is initially collected onto multibed (Tenax TA/Graphitized Carbon/Carboxen 1000),
445   preconditioned glass sorbent tubes that are optimized for $C_{2/3}$–C_{30} species. The first stage of
446   trapping allows sampling rates up to 100 sccm, followed by forward-flushing with UHP nitrogen
447   to remove water. For the higher volatility channel (Channel 1), additional H_2O was removed from
448   the ambient sample stream via passing through a cooled PFA tube (1/8-inch O.D., 1/16-inch I.D.,
449   3.375-inch length, 15°C) prior to trapping of VOCs to avoid water condensed in the sample tube.
450   After the initial collection and water purge, the sample was then transferred to the focusing stage,
451   which is a multibed (Tenax, Carbopack X, Carboxen 1003) glass cold trap. After preconcentration,
452   the samples are transferred to different separation columns (Restek Rt-Q-Bond and Rxi-624) for
453   Channels 1 and 2, respectively. Channel 1 is optimized for separation of C_3-C_4 alkanes, C_1-C_2
454   halocarbons and C_1-C_3 oxygenates; Channel 2 is optimized for C_5-C_{12} alkanes, C_6-C_{10} aromatics,
455   C_3-C_6 oxygenates.

457   The GC inlet consisted of approximately 8 m of 0.25-inch O.D., 0.15625-inch I.D. PFA tubing
458   connected to a sample pump, with an inlet flow of approximately 1 slpm. The GC pulled a sub-
459   flow from the main GC inlet via 1-m length, 0.125-inch O.D., 0.0625-inch I.D. PFA tubing. The
460   sample flow was 80 sccm to each GC channel for 10 minutes during each 30-minute analytical
461   cycle. Before preconcentration, the ambient sample is passed through a bed of pre-cleaned sodium
462   sulfite (nominal 1 g) to scrub ozone and thereby reduce sampling artifacts [Helmig, 1997].

464   The TDPC employed for this campaign relied upon two-stage adsorbent trapping for
465   preconcentration of analytes. The sample is initially collected onto multibed (Tenax
466   TA/Graphitized Carbon/Carboxen 1000), preconditioned glass sorbent tubes that are optimized for
467    $C_{2/3}$–C_{30} species. The first stage of trapping allows sampling rates up to 100 sccm, followed by
468   forward-flushing with UHP nitrogen to remove water. For the higher volatility channel (Channel
469   1), additional H_2O was removed from the ambient sample stream via passing through a cooled
470   PFA tube (1/8-inch O.D., 1/16-inch I.D., 3.375-inch length, 15°C) prior to trapping of VOCs to
471   avoid water condensed in the sample tube. After the initial collection and water purge, the sample
472   was then transferred to the focusing stage, which is a multibed (Tenax, Carbopack X, Carboxen
473   1003) glass cold trap.

475   Calibration was performed by multicomponent VOC calibrant gas (Apel-Riemer Environmental
476   Inc., Miami, FL, USA) diluted in UHP N2 at sufficient total flow to overflow the GC sub-inlet.
477   Instrument calibrations were performed in-field each night throughout the campaign via automated
478   valve switching. Note that this calibration mixture was the same as described in Section 2.2.3.

3. Results

482   The following sections outline PTR-ToF-MS interferences observed for ions typically assigned to
483   isoprene, oxygenated VOCs, and aromatic VOCs. The primary data used for this analysis are from
484   the NOAA PTR-ToF-MS, which provided direct evidence of interferences via GC pre-separation.
485   Each section begins with a description of GC-PTR-ToF-MS samples collected along the Las Vegas
486   Strip during SUNVEx. This region comprises many hotels and entertainment establishments and
487   is impacted by emissions from fossil fuels, VCPs, and restaurant cooking. This region had the
488   highest observed mixing ratios compared to New York, Detroit, and Los Angeles. These
489   interferences are then compared to ground site data collected by the NOAA PTR-ToF-MS during

490   SUNVEx/RECAP-CA. Finally, other observations are used to show the ubiquity of these
491   interferences across instruments and urban environments. A key focus of this discussion is the
492   impact of fragmentation on PTR-ToF-MS observations of m/z 69 (exact mass 69.070), which is
493   typically assigned to isoprene. We also focus on methods to determine urban isoprene mixing
494   ratios when fragmentation from other higher molecular weight molecules is important.
495
496   **3.1.   Isoprene**
497
498   **3.1.1. Known interferences to isoprene (m/z 69)**
499

500   Biogenic VOCs are commonly reported by PTR-ToF-MS, including isoprene and the sum of
501   monoterpene isomers. Isoprene is the dominant biogenic VOC emitted by urban foliage and is a
502   major contributor to urban OH reactivity (Calfapietra et al., 2013). Interferences to isoprene in
503   PTR-ToF-MS spectra results from the production of the $C_5H_8H^+$ ion, which is a common fragment
504   for higher-carbon aldehydes (> C_5), alkenes, and cycloalkanes (Buhr et al., 2002;Gueneron et al.,
505   2015;Pagonis et al., 2019;Romano and Hanna, 2018). Previous studies have characterized ambient
506   isoprene interferences from 2-methyl-3-buten-2-olalkenes emitted from biogenic sources (e.g.,
507   Karl et al., 2012) and cycloalkanes emitted from fossil fuels use and oil and natural gas production
508   (e.g., Gueneron et al., 2015;Warneke et al., 2014;Pfannerstill et al., 2023). For example, Gueneron
509   et al. (2015) showed that substituted cyclohexanes and cyclohexenes produce fragmentation
510   patterns that consist largely of m/z 111, m/z 125, m/z 69, m/z 83, m/z 57, and other lesser-abundant
511   hydrocarbon fragments. In regions with significant oil and natural gas development, these
512   compounds may produce interferences at m/z 69 which can interfere with the signal resulting from
513   biogenic sources of isoprene (e.g., Warneke et al., 2014). Similarly, Kilgour et al. (2021) show
514   that aldehydes emitted due to ozone deposition to surface ocean waters may interfere with the
515   quantification of isoprene. The key aldehydes observed to produce an interference were nonanal
516   and octanal. The same aldehydes may be produced on inlet surfaces exposed to high ozone
517   concentrations and result in an isoprene artifact (Ernle et al., 2023;Vermeuel et al., 2022).
518
519   **3.1.2. Characterizing aldehyde interferences to m/z 69 using GC-PTR-ToF-MS**
520

521   Figure 2 shows a GC-PTR-ToF-MS chromatogram of the ion typically assigned to isoprene (m/z
522   69, $C_5H_8H^+$). This sample was collected on the Las Vegas Strip in the evening (~ 22:15 local time,
523   LT) when biogenic emissions of isoprene are expected to be low. The chromatogram shows that
524   isoprene (retention time, RT = 65 s) is only a small contributor to the signal at m/z 69 measured in
525   this region. Additional peaks are observed at RT = 210 s, 250 s, 600 s, and 710s. These peaks are
526   not cycloalkanes, as might be expected from mobile source emissions (Gueneron et al., 2015);
527   rather, these are dehydration and fragmentation products of saturated aldehydes, including
528   methylbutanal, pentanal, octanal, and nonanal. Chromatograms of the parent ions attributed to
529   octanal and octanone (m/z 129, $C_8H_{16}OH^+$), together with nonanal and nonanone (m/z 143,
530    $C_9H_{18}OH^+$) are shown in Fig. S3. The parent ion and the dehydration products (m/z 111 $C_8H_{15}^+$
531   and m/z 125 $C_9H_{17}^+$, respectively) are observed, but at different ratios between the aldehydes and
532   ketones. Pentanal and methylbutanal almost entirely dehydrate and do not exhibit significant signal
533   at the parent ion mass. Comparisons of ambient observations with GC-PTR-ToF-MS
534   chromatograms of standard mixtures show that only aldehydes (and not the ketones) are observed
535   in significant quantities on the Las Vegas Strip (Fig. S3).

13

536
537
538
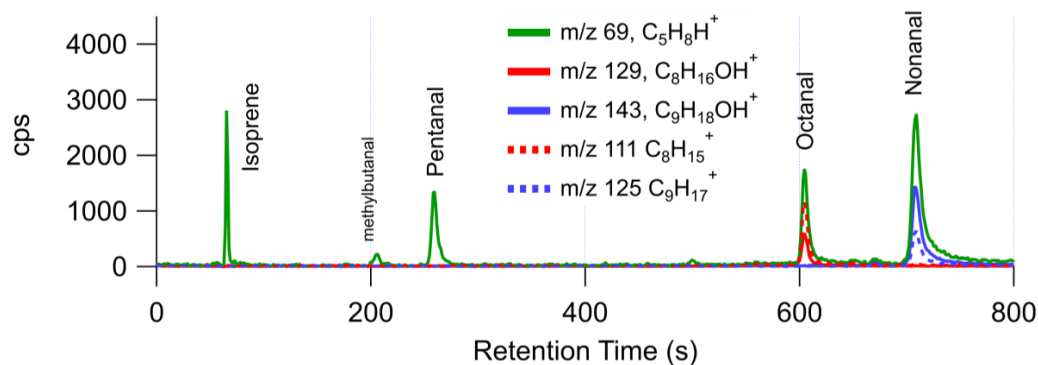
539
540 **Figure 2.** GC-PTR-ToF-MS chromatogram from downtown Las Vegas at 22:15 on 30 July 2021, showing the
541 contributions of isomers and fragments to the ion typically assigned to isoprene (m/z 69, $C_5H_8H^+$).

542

543 These aldehydes emissions likely result from cooking (Arata et al., 2021;Klein et al., 2016;Schauer
544 et al., 1999;Karl et al., 2018;Wernis et al., 2022) and their significant presence on the Las Vegas
545 Strip possibly reflects the high density of restaurants along Las Vegas Boulevard. Figure 3 shows
546 mobile laboratory measurements of nonanal and m/z 69 during evening drives on 28 June and 30
547 July 2021. GC-PTR-ToF-MS sampling was only conducted on 30 July and the location of the
548 sample (Las Vegas Strip) is shown in Fig. 1a. During both drives, m/z 69 was enhanced along Las
549 Vegas Boulevard and mixing ratios reached a maximum of 6 ppb (assuming a sensitivity
550 equivalent to isoprene). On 28 June, m/z 69 and nonanal detected at m/z 143 ($C_9H_{18}OH^+$) are
551 highly correlated ($r^2 > 0.93$), suggesting that these ions share a common source. A similar
552 correlation was observed between m/z 69 and octanal ($r^2 = 0.90$).

553
554
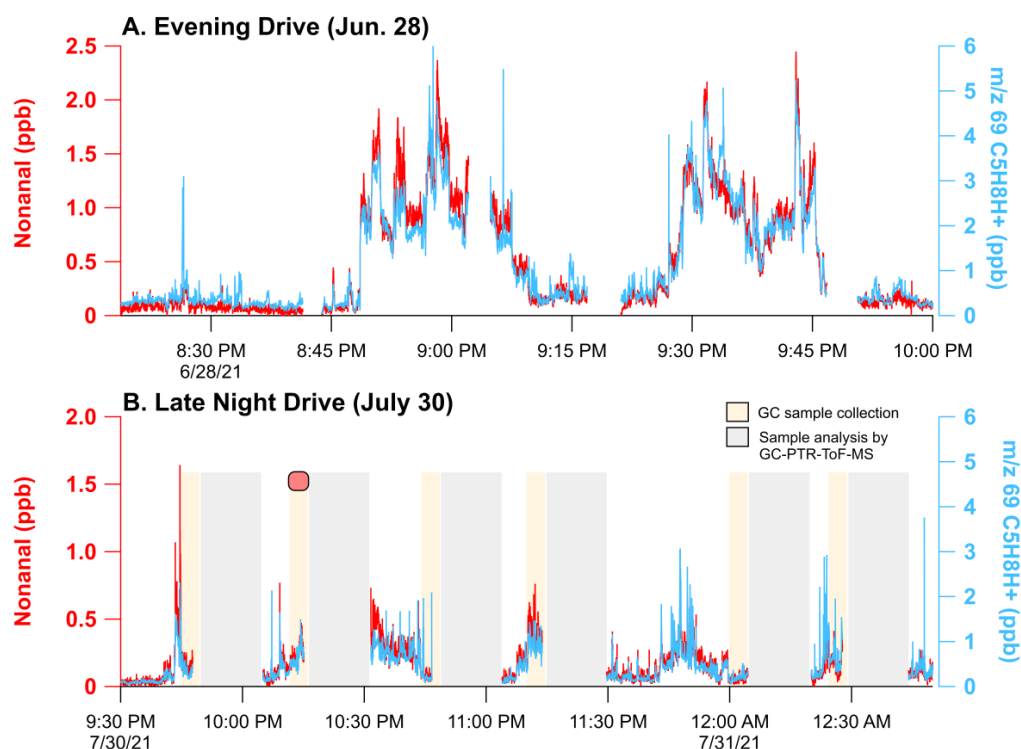
Figure 3. Mobile laboratory data showing PTR-ToF-MS measurements of nonanal (m/z 143, $C_9H_{18}OH^+$, red) and m/z 69 ($C_5H_8H^+$, blue) on the Las Vegas Strip during nighttime hours on (a) 28 June and (b) 30 July 2021. GC samples were only collected on 30 July, and the shaded regions in (b) show periods of sample collection (beige) and sample analysis (grey). The red marker in (b) indicates the time of the GC-PTR-ToF-MS sample shown in Fig. 2.

Long-chain aldehydes are not routinely reported in urban datasets and the isoprene interference due to aldehyde fragmentation is underappreciated in ambient PTR-ToF-MS datasets. Studies have described how aldehydes produced on the surfaces of inlet tubing interfere with isoprene measured by PTR-ToF-MS in remote forests (Vermeuel et al., 2022) and in the stratosphere (Ernle et al., 2023), and aldehydes emitted from ocean surface waters also interfere with isoprene measurements in laboratory studies and ambient measurements near coastal regions (Kilgour et al., 2021). Long-chain aldehydes are likely ubiquitous in cities, and cooking activities are likely a major source of octanal and nonanal resulting in an isoprene interference (Wernis et al., 2022;Peng et al., 2022).

The interference from aldehydes is likely common across PTR designs, even though differences could exist due to operating conditions (e.g., the E/N ratio). Figure S1 compares the fragmentation patterns of pentanal, octanal, and nonanal observed in the NOAA PTR-ToF-MS (E/N ~ 140 Td), which utilizes the Vocus ion source, to those reported by Buhr et al. (2002) (E/N ~120–130 Td), which employ a traditional drift tube and quadrupole. In both reactor designs, C_5-aldehydes dehydrate to produce $C_5H_8H^+$ (m/z 69) directly, while larger aldehydes such as octanal and nonanal dehydrate to produce $C_8H_{15}^+$ (m/z 111, exact mass: 111.117) and $C_9H_{17}^+$ (m/z 125, exact mass: 125.123), then further fragment to produce the $C_5H_8H^+$ ion (Buhr et al., 2002;Pagonis et al., 2019).

579 These dehydration products are unique to aldehydes since ketone isomers do not undergo
580 significant fragmentation (Fig. S3).
581
582 We note that even though the fragmentation was similar between two instruments with different
583 reactor designs, fragmentation may result from the operation of other instrument components. For
584 example, the intensity of aldehyde fragmentation was found to vary strongly with voltage gradients
585 within the BSQ of the Berkeley Vocus-PTR-ToF-MS (Fig. S2). These results show that PTR-ToF-
586 MS systems employing quadrupole ion guides may exhibit fragmentation outside of the drift tube
587 region; consequently, care may be needed when tuning instruments to minimize unwanted
588 secondary reactions.
589
590 **3.1.3. Corrections to ground site observations of m/z 69 in Los Angeles and Las Vegas**
591
592 GC-PTR-ToF-MS and mobile laboratory measurements described in Section 3.1.2 indicate that
593 aldehydes significantly contribute to the signal at m/z 69 in urban areas. Chromatograms show that
594 the dehydration products from nonanal (m/z 125) and octanal (m/z 111) are useful markers that
595 distinguish aldehydes from ketone isomers. Coincidentally, the dehydration products from nonanal
596 and octanal are identical to the fragments produced from substituted cyclohexanes, which interfere
597 with isoprene in hydrocarbon-rich environments (see Gueneron et al., 2015;Warneke et al.,
598 2014;Pfannerstill et al., 2023). Here, it is proposed that the signals at m/z 111 and m/z 125 can be
599 used as proxies to calculate the contribution from aldehyde and cycloalkane fragmentation on the
600 signal at m/z 69 in urban areas.
601
602 Figure 4 shows how the sum of m/z 111 and m/z 125 (termed the "isoprene interference") varies
603 relative to the signal at m/z 69 measured at the ground sites in Los Angeles and Las Vegas. In Los
604 Angeles, high daytime emissions of isoprene dominate and comprise most of the signal of m/z 69
605 from 6:00–19:00 LT. The high variability in the signal at m/z 69 is caused by very localized
606 emissions from trees upwind of the measurement site. In Las Vegas, isoprene emissions are much
607 lower and the diel pattern of m/z 69 closely follows the behavior of the isoprene interference with
608 only small additional signal during the daytime.
609
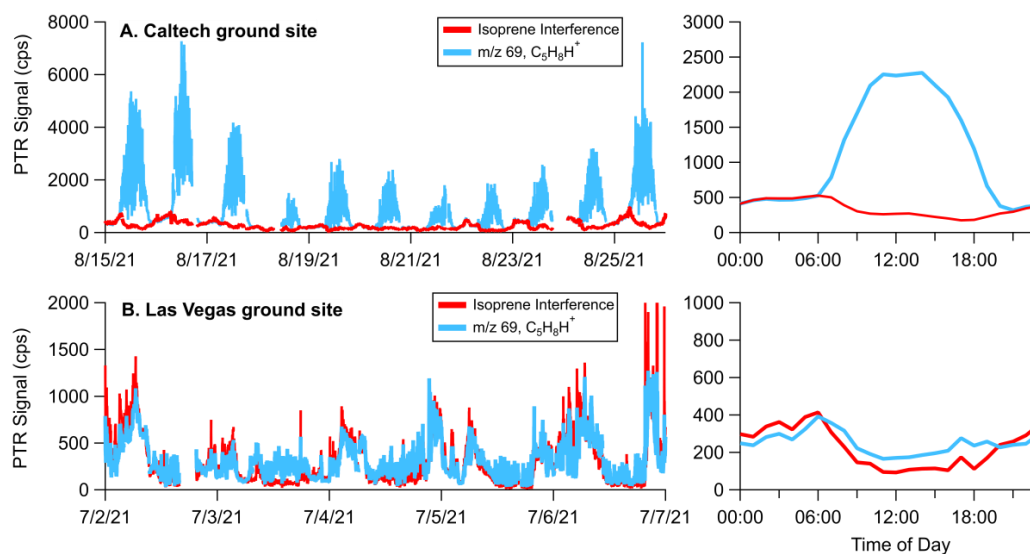
Figure 4. Time series and diurnal pattern of the signal at m/z 69 ($C_5H_8H^+$) and the isoprene interference (m/z 111 + m/z 125) measured at (a) the Caltech ground site and (b) the Las Vegas ground site. The time series data are shown for select periods to illustrate correlations between the isoprene interference and m/z 69. The diel patterns on the right are campaign averages.

Biogenic isoprene is predominantly emitted during daytime hours (e.g., Guenther et al., 2012), while the isoprene interference in both cities is more prevalent at night. These differences in diurnal patterns can be leveraged to subtract interferences from aldehydes and cycloalkanes from PTR-ToF-MS measurements of m/z 69. Here, the signals at m/z 69, m/z 111, and m/z 125 are analyzed between 00:00-04:00 LT when daytime isoprene from biogenic sources is expected to be low. The instrument response to aldehyde and cycloalkane fragmentation is calculated by determining the ratio of m/z 69 to the sum of m/z 111 + m/z 125. This ratio is then applied to the full dataset following Eq. 1.

$$\text{m/z } 69_{\text{Corrected}} \ = \ S_{69} - S_{111+125} \cdot f_{69/(111+125)} \ \text{(Eq. 1)}$$

S_{69} is the signal measured at m/z 69, $S_{111+125}$ is the signal of the isoprene interference (sum of m/z 111 + m/z 125), and $f_{69/(111+125)}$ is the interference ratio determined at night. The nighttime interference ratio is 3.0 in Las Vegas and 3.5 in Los Angeles (Fig. S4). The differences between the cities may reflect variations in the distribution of aldehydes and cycloalkanes.

Figure 5 shows how measurements of m/z 69 change as a result of this correction and compares the corrected/calculated isoprene mixing ratios to the GC-MS measurements co-located with the PTR-ToF-MS. In Los Angeles, the correction largely impacts m/z 69 signals at night. The diurnal pattern shows that average mixing ratios approach zero in the evenings, though increases in nighttime isoprene mixing ratios are observed during some periods (e.g., 22–24 August, Fig. S5). Corrections to m/z 69 during the daytime lead to a ~ 10% decrease in reported mixing ratios. This shows that even when isoprene emissions are high, VOC fragmentation can have a significant impact on the signal at m/z 69.

641
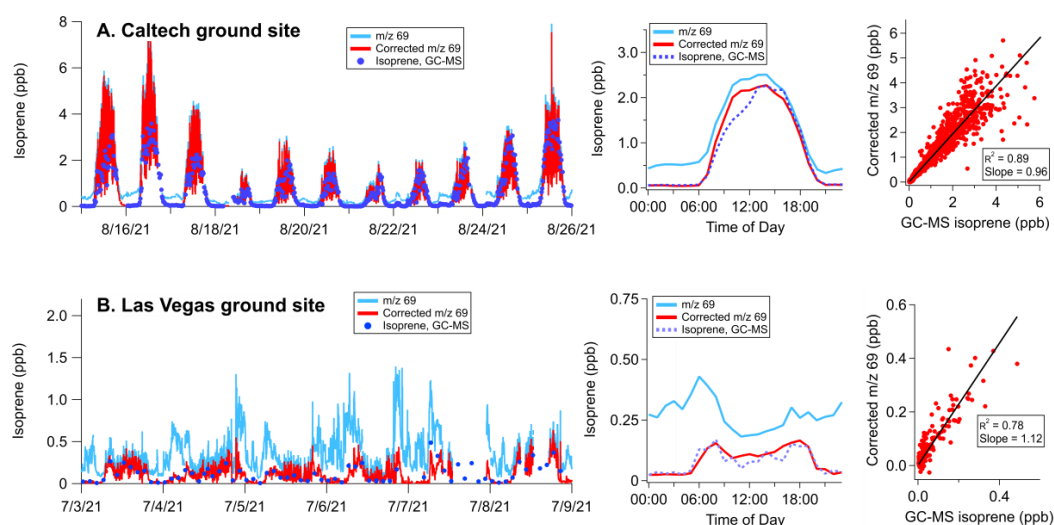
642
643 **Figure 5**. Uncorrected and corrected m/z 69 as time series, diel averages, and correlation plots for (a) the Caltech and
644 (b) Las Vegas ground sites. GC-MS measurements are shown for comparison against the corrected m/z 69 isoprene
645 mixing ratios. A detailed comparison of nighttime isoprene corrections in Los Angeles is shown in Fig. S5.

646
647 The corrected m/z 69 measurements are well correlated with GC-MS isoprene measurements (r^2
648 = 0.89) and agree to within 4%. At high isoprene mixing ratios, the measurements exhibit a greater
649 degree of scatter. This variability likely results from the differences in sampling timescales (1 s for
650 PTR-ToF-MS, ~ 120 s for GC-MS) along with the high variability of isoprene emissions from
651 trees at the measurement site. When averaged to a diel profile, the daytime mixing ratios also agree
652 to within 4%. Both instruments show that average isoprene decreases to low mixing ratios at night
653 (< 0.05 ppb). The GC-MS observed a number of periods of enhanced nighttime isoprene, likely
654 from non-biogenic sources. Remarkably, after accounting for the isoprene interference, the
655 corrected m/z 69 mixing ratios from the PTR-ToF-MS captures the variability in nighttime
656 isoprene observed by GC-MS in Los Angeles (Fig. S5). On average, the isoprene interference
657 represents ~90% of the nighttime signal of m/z 69.

658
659 The isoprene correction is most impactful on the Las Vegas measurements where isoprene
660 emissions are low and aldehydes + cycloalkane fragments constitute a larger fraction of the signal
661 at m/z 69. Without correction, the variability in m/z 69 across all daytime hours is driven by the
662 isoprene interference (Fig. 4). After the interference contributions are subtracted, corrected
663 isoprene mixing ratios approach zero at night and decrease by nearly 50% to 0.1–0.15 ppb during
664 the day (Fig. 5b). The resulting diel pattern changes substantially and exhibits a daytime peak that
665 is consistent with the expected pattern for isoprene. GC-MS measurements show that isoprene
666 mixing ratios were typically < 0.2 ppb and the corrected m/z 69 diel pattern generally matches the
667 average diel pattern of isoprene reported by GC-MS. Though the number of canister samples in
668 Las Vegas were limited (total 275, sampled every 2–4 h), a comparison between the corrected m/z
669 69 and GC-MS isoprene shows that the measurements agree to within 15%.

670
671 **3.1.4. Corrections to aircraft measurements of m/z 69 over Los Angeles**

672

673 The isoprene interferences observed during SUNVEx and RECAP-CA show that PTR-ToF-MS
674 measurements of m/z 69 are significantly impacted by aldehydes and cycloalkanes. To assess the
675 impact of isoprene interferences at higher altitudes, we analyze the FIREX-AQ and RECAP-CA
676 measurements of flights in the Los Angeles Basin and determine corrected m/z 69 signals
677 following Eq. (1). One challenge to this approach is that the DC-8 and Twin Otter aircraft did not
678 sample the Los Angeles Basin at night, and therefore the interference ratio ($f_{69/(111+125)}$) is not easily
679 determined in the absence of isoprene. To overcome this limitation for FIREX-AQ, we vary the
680 interference ratio until the corrected m/z 69 signals reported by the NOAA PTR-ToF-MS matches
681 with the isoprene mixing ratios reported by GC instrumentation on the DC-8. The resulting ratio
682 determined by iteration (4.4) is ~ 20% higher than the ratio determined at ground level during
683 SUNVEx (3.5), which likely reflects differences between the operating conditions and drift tube
684 designs used on the NOAA PTR-ToF-MS during FIREX-AQ and SUNVEx (traditional vs.
685 Vocus).

686

687 Figure 6 illustrates the spatial and temporal variability in (a) the corrected m/z 69 mixing ratios
688 and (b) the calculated interference. Transits to the north show that the interference is highest along
689 the San Gabriel Mountains where anthropogenic pollution typically builds in the Los Angeles
690 Basin (Angevine et al., 2013) and reached mixing ratios as high as 500 ppt. The interference
691 correlates well with both methylcyclohexane measured by the UCI WAS and methylpropanal
692 measured by TOGA-TOF, which are proxies for the species known to fragment to produce the
693 isoprene interference (i.e., cycloalkanes and aldehydes). Corrected m/z 69 mixing ratios only
694 exhibit significant enhancements in regions where the DC-8 sampled air close to vegetation. Short
695 bursts of isoprene were observed above the San Gabriel Mountains, but mixing ratios were
696 typically lower than 500 ppt. Over the entire flight, the isoprene interference constituted > 50% of
697 the signal observed at m/z 69.

698

699 Figure 6c compares the PTR-ToF-MS measurements to GC-based samples for uncorrected m/z 69
700 (top) and corrected m/z 69 mixing ratios (bottom). These comparisons show that the isoprene
701 interference resulted in an overestimation of PTR-ToF-MS measurements of isoprene by at least a
702 factor of 2. At times, the NOAA PTR-ToF-MS measured mixing ratios of m/z 69 that were 5 times
703 larger than the isoprene mixing ratios reported by GC-based methods. The Oslo PTR-ToF-MS also
704 sampled onboard the DC8 during FIREX-AQ and presented an opportunity to compare to the
705 fragmentation observed by the NOAA PTR-TOF-MS. Following a similar correction procedure as
706 described above, Fig. S6 shows that the Oslo PTR-ToF-MS measured the same degree of
707 interferences as the NOAA PTR-ToF-MS (i.e., fragmentation biased isoprene measurements high
708 by at least a factor of 2). The consistency between both instruments demonstrates that isoprene
709 interferences are common across PTR-ToF-MS designs (i.e., Tofwerk vs. Ionicon).
710
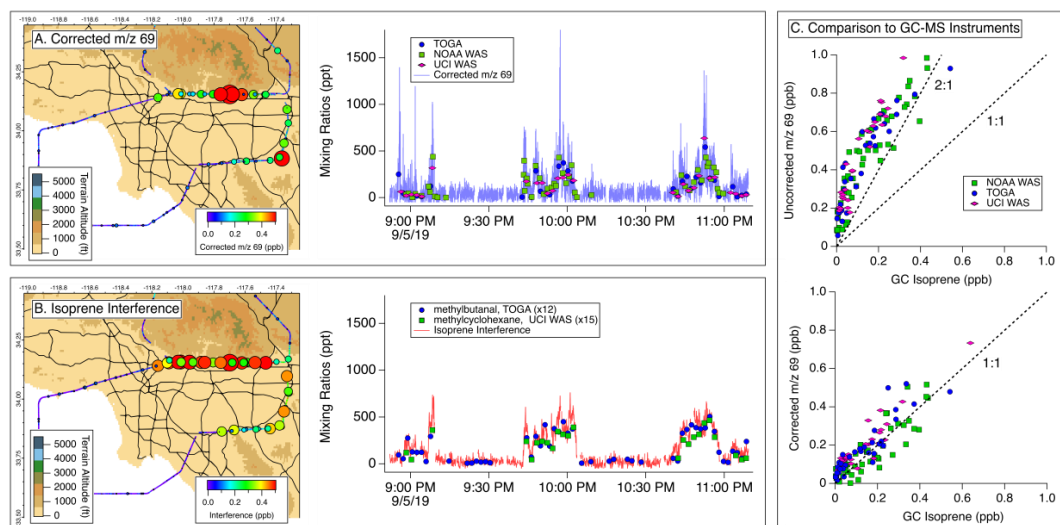
Figure 6. Impact of isoprene interference correction on m/z 69 measurements from the NOAA PTR-ToF-MS during FIREX-AQ. (a) Map of corrected m/z 69 distribution (left) and time series with corresponding measurements of isoprene from GC-MS samples (right). (b) Map of isoprene interference (left) and time series with GC-MS measurements of methylcyclohexane and methylpropanal, which are proxies for cycloalkanes and aldehydes known to contribute to the signal at m/z 69. (c) Comparisons of PTR-ToF-MS measurements of m/z 69 and GC-based isoprene mixing ratios for uncorrected m/z 69 (top) and corrected m/z 69 (bottom) using Eq. (1) with an interference ratio = 10.

The Berkeley Vocus PTR-ToF-MS also observed interferences to m/z 69 during the RECAP-CA flights. Unlike FIREX-AQ, GC-MS measurements were not available onboard the Twin Otter to compare against PTR-ToF-MS measurements. To evaluate the interference contributions to m/z 69 here, we determine the interference ratio from nonanal calibrations and compare it with data collected from the Central Valley and Los Angeles Basin. In these regions, the signal at m/z 69 and the sum of m/z 111 + 125 are well-correlated with a slope that closely matches the measured fragmentation pattern for nonanal (Fig. S7). The interference ratio observed in the Central Valley where oil and natural gas emissions are significant is similar to the ratio observed in Los Angeles where aldehydes are more important. In the Central Valley, periods of high biogenic influence are clearly separated from periods of high interference from anthropogenic emissions. Building on these responses, we use the calibrated data for nonanal to derive an m/z 69 correction in Los Angeles. This method is limited in accounting for molecules that have fragmentation ratios differing from nonanal, but since the interference ratio observed from oil and gas regions and from the Los Angeles Basin is similar to the nonanal fragmentation ratio, we expect the uncertainty to be relatively small despite there being no GC comparison.

Figure 7 shows the impact of the isoprene interference on the Berkeley PTR-ToF-MS data. The Twin Otter flew nine flights and the total signal of m/z 69 varied between 200–1200 ppt. Similar to the observations by the NOAA PTR-ToF-MS during FIREX-AQ, the isoprene interference during RECAP-CA was at least 50% of the signal observed at m/z 69 (Fig. 7c). The Twin Otter sampled a larger swath of area than the DC-8, and Fig. 7 shows that the interference is persistent across the Los Angeles Basin (Fig. 7b) at mixing ratios as high as 600 ppt. Similar to the DC-8 flight, corrected m/z 69 mixing ratios are highest along the San Gabriel Mountains. The Twin Otter

743 is capable of sampling at lower altitudes than the DC-8, and therefore larger mixing ratios of
744 isoprene were observed.
745
746
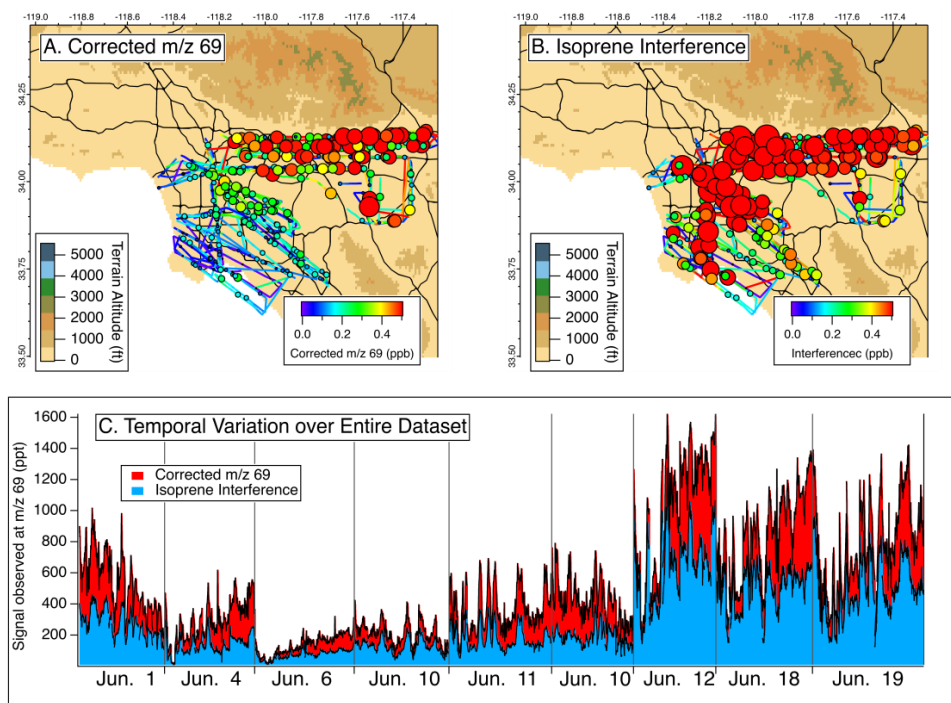
747
748 **Figure 7.** Impact of isoprene interference correction on isoprene measurements during RECAP-CA as (a) the corrected
749 isoprene distribution, (b) the isoprene interference, and (c) a pseudo time series of the total m/z 69 signal colored by
750 the contributions of corrected m/z 69 and isoprene interference for all flights.
751

752 The contribution of the isoprene interference observed from the aircraft with the Berkeley PTR-
753 ToF-MS differs from the observations at Caltech during RECAP-CA. On the ground, the isoprene
754 interference was ~10% of the signal at m/z 69 during daytime hours (Fig. 5a), while at altitude it
755 was > 50%. This difference can be explained by (1) the abundance of isoprene emitters close to
756 the ground site, (2) the differences in reactivities between isoprene, aldehydes, and cycloalkanes,
757 and (3) the different instrument setting of the Berkeley PTR-ToF-MS (Fig. S2). Isoprene is highly
758 reactive towards atmospheric oxidants such as the OH radical (k_{OH} ~ 1×10^{-10} cm^3 molecule^{-1} s^{-1}
759), whereas saturated aldehydes and cycloalkanes are expected to be 5–10 times less reactive
760 (Burkholder et al., 2019). This difference in reactivity may alter the distribution of VOCs that
761 contribute to m/z 69 and result in higher interferences aloft. The DC-8 and Twin Otter aircraft did
762 not specifically target altitude profiling while sampling in the Los Angeles Basin, but future work
763 may help to characterize the impact of the isoprene interference at other altitudes.
764

765 **3.1.5. Corrections to m/z 69 measured in Detroit, MI**
766

767 The SUNVEx/RECAP-CA/FIREX-AQ data reflect the behavior of the NOAA, Oslo, and Berkeley
768 instruments during summertime measurements in Los Angeles. Isoprene interferences likely

impact ground and airborne measurements in other cities and at other times of year. Figure 8 shows the impact of interferences to the signal at m/z 69 reported by the Aerodyne PTR-ToF-MS measurements during MOOSE. This campaign targeted emissions in Detroit, MI, where the Aerodyne Mobile Laboratory conducted a mix of mobile and stationary sampling in select locations around the metropolitan area (Fig. 1). Figure 8a shows a subset of PTR-ToF-MS measurements of m/z 69 and corrected m/z 69, along with isoprene measurements by the Aerodyne GC-MS. Corrected m/z 69 is calculated by determining the interference ratio at night (= 2.54), similar to the approach used to calculate interferences during SUNVEx/RECAP-CA. Figure 8b shows normalized histograms for each measurement over the entire deployment.
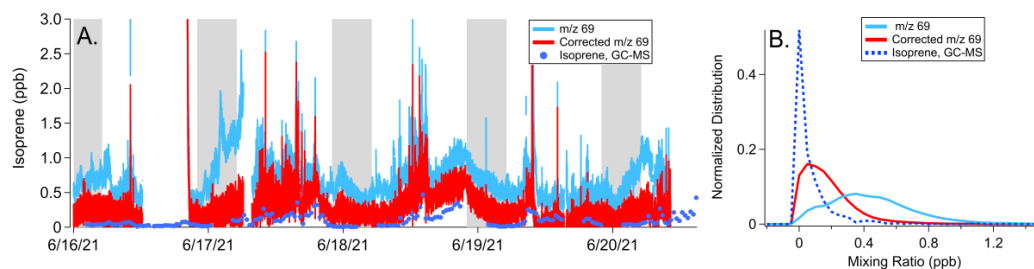
Figure 8. Impact of isoprene interference correction on the PTR-ToF-MS data collected from the Aerodyne Mobile Laboratory during the MOOSE campaign as a (a) time series of GC-MS measurements, uncorrected and corrected m/69 isoprene mixing ratios. The shaded regions show nighttime measurements (22:00–05:00 LT). (b) Histograms showing the distribution of m/z 69 measured by the Aerodyne PTR-ToF-MS, corrected m/z 69 isoprene mixing ratios, and isoprene mixing ratios measured by the GC-MS.

Without correction, m/z 69 reported by PTR-ToF-MS exhibits a broad distribution with a peak mixing ratio of ~ 0.4 ppb (Fig. 8b). After applying the corrections described by Eq. (1), m/z 69 signals decrease by nearly a factor of 2 and show better agreement with isoprene reported by GC-MS. Corrected m/z 69 mixing ratios are still a factor of 2 higher than the isoprene mixing ratios reported by the GC-MS. One possibility is that other VOCs in the Detroit region may also contribute to the signal at m/z 69. GC pre-separation measurements directly using PTR-ToF-MS were not conducted during MOOSE; consequently, it is difficult to determine what other species might contribute to m/z 69 in this region. Broad deployment of GC-PTR-ToF-MS measurements in urban areas may help to better quantify the contributions of fragmenting species to PTR-ToF-MS measurements of m/z 69.

3.1.6. Seasonal changes to the m/z 69 interferences observed in New York City

Figure 9 shows the impact of the isoprene interference on data reported by the Stony Brook PTR-ToF-MS during a year-long sampling effort to characterize emissions in New York City during the COVID-19 lockdown. Shown here are mixing ratios of m/z 69 along with the estimated contribution to m/z 69 from the isoprene interference. We calculate the isoprene interference for each season, and present the diurnal patterns in the top row. The interference ratio ($f_{69/(111+125)}$, Eq. (1)) is similar in spring, summer, and winter (2.2–2.5), but lower during fall (1.9).
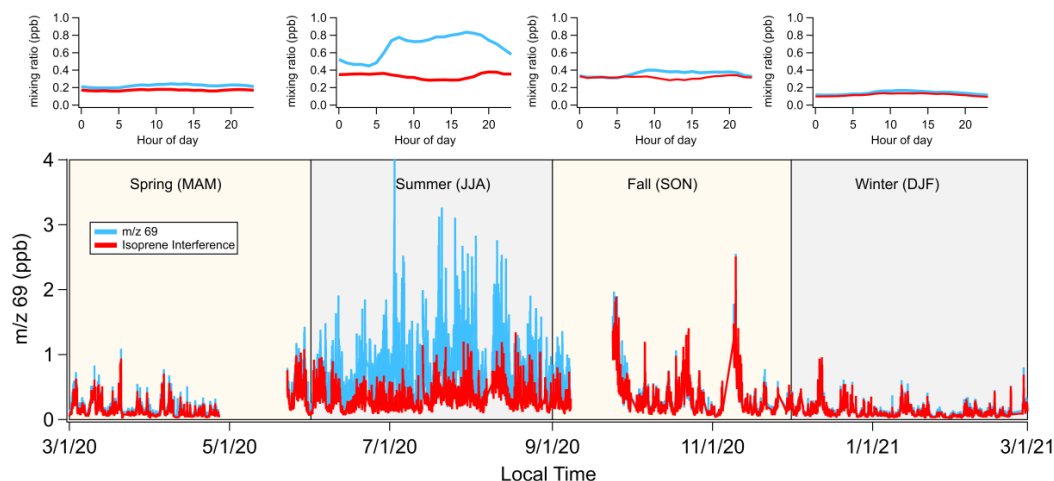
Figure 9. (bottom) Time series of m/z 69 and isoprene interference measured by the Stony Brook PTR-ToF-MS at the urban ASRC ground site in New York City. (top) Diel patterns of m/z 69 and isoprene interference mixing ratios for each season.

The signal at m/z 69 is variable across seasons and the highest mixing ratios are observed during summer. The isoprene interference is a major contributor to m/z 69 in fall, winter, and spring (77-88% of total signal) and strongly influences the day-to-day variability. During summertime isoprene emissions from urban foliage increases the variability in m/z 69 and results in higher mixing ratios of m/z 69 during the day. The isoprene interference increases the background mixing ratios of m/z 69 and dominates the total signal at night.

The ASRC site is located in a heavily urbanized region and the PTR-ToF-MS sampled air at the top of the building where mixing ratios of isoprene are likely lower. The persistent, high contribution from the isoprene interference to m/z 69 during all seasons likely reflects the high emissions of aldehydes and cycloalkanes from anthropogenic sources in this region. Figure S8 contrasts the measurements at ASRC with those reported from the Flax Pond site. Flax Pond is located in a less-densely populated region of Long Island where biogenic sources of isoprene are more abundant. There, interferences are a much smaller fraction of the signal at m/z 69 ($< 10\%$) and the variability is largely driven by isoprene during the summer months. Mixing ratios at Flax Pond are lower during the winter, but comparable to those observed at ASRC during the same season (~ 100-150 ppt). Furthermore, the variability is predominantly driven by the isoprene interference. Figures 9 and S8 demonstrate that interferences will vary spatially between heavily urban and biogenic-dominated regions. In addition, outside of the summer months, isoprene is unlikely to be a major contributor to m/z 69 in both regions.

The contribution of the isoprene interference to m/z 69 in New York City is comparable to the ground level measurements in Las Vegas, Los Angeles, and Detroit (0.25–0.5 ppb), which demonstrates that isoprene measurements by PTR-MS are likely to be significantly impacted across most, if not all, urban regions. Identifying anthropogenic or nighttime sources of isoprene by PTR-MS will be difficult if not confirmed unambiguously by GC-PTR-ToF-MS or separately by GC-MS.

3.2. Oxygenated VOCs

3.2.1. Characterizing interferences to oxygenated VOCs using GC-PTR-ToF-MS

Small oxygenated VOCs are an important contributor to the reactivity and ozone produced in urban areas. Alcohols, ketones, and small aldehydes ($< C_4$) may be emitted to the atmosphere from mobile sources, VCPs, cooking activities, and other sources (Klein et al., 2016;McDonald et al., 2018), but are also formed as secondary products of atmospheric chemistry. Some studies have reported that certain alcohols, such as ethanol, may ionize to product products that overlap with proton-transfer products of other important oxygenates, such as acetaldehyde (Buhr et al., 2002;Pagonis et al., 2019). Previous intercomparisons have shown that acetaldehyde is one example of oxygenated VOCs where there may be large disagreements between PTR-ToF-MS and GC-MS (Yuan et al., 2016).

Figure 10 shows the GC-PTR-ToF-MS chromatogram collected on the Las Vegas Strip for proton-transfer products typically assigned to oxygenated VOCs. Here, we present small oxygenates typically reported in ambient data sets that are subject to fragmentation or interferences, including methanol, acetaldehyde, ethanol, and C_4-carbonyls, which represent the sum of methacrolein (MACR), methyl vinyl ketone (MVK), and crotonaldehyde.

First, GC-PTR-ToF-MS data show that no other species elute through the GC column to yield a significant interference to methanol and ethanol. The signal at m/z 59 ($C_3H_6OH^+$) is also observed to result entirely from acetone + propanal (not shown). This is consistent with previous studies that show good agreement between GC-MS and PTR-ToF-MS (e.g., Warneke et al., 2003).

Crotonaldehyde is a major fraction of the C_4-carbonyls observed on the Las Vegas Strip. Typically, MVK and MACR are treated as the dominant isomers to the C_4-carbonyl product (m/z 71, $C_4H_6OH^+$), since these are secondary products from isoprene oxidation and are expected to be present at high mixing ratios (Yuan et al., 2017). Crotonaldehyde is observed to be a major contributor to m/z 71 in biomass burning emissions (Koss et al., 2018), but its presence on the Las Vegas Strip likely points to other important aldehyde sources, such as cooking. The higher fraction of crotonaldehyde reflects that isoprene mixing ratios are lower in Las Vegas than other cities (Fig. 5) and that cooking is an important source of VOCs along the Las Vegas Strip (Fig. 2). Xu et al. (2022) showed that measurements of C_4-carbonyls by the NOAA PTR-ToF-MS, ammonium-adduct chemical ionization mass spectrometer (NH_4-CIMS), and NOAA GC-MS agreed in the daytime during RECAP-CA when MVK and MACR were high, but disagreed at night when isoprene products were low and crotonaldehyde mixing ratios were likely elevated. Additional interferences at m/z 71 could result from decomposition of ISOPOOH on inlet surfaces (Rivera-Rios et al., 2014).
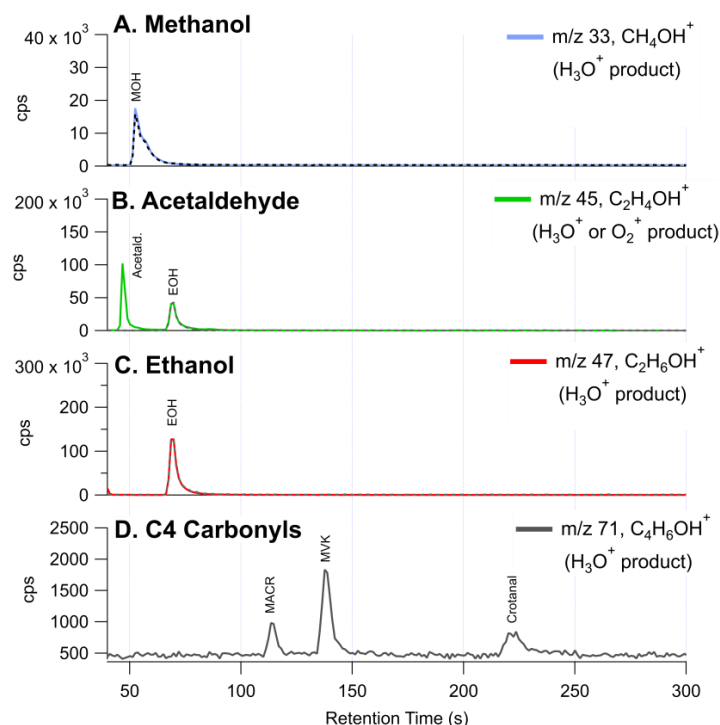
Figure 10. GC-PTR-ToF-MS chromatograms from the Las Vegas Strip showing the contributions of isomers and fragments to ions typically assigned to small oxygenates. The labels highlight the traditionally assigned isomers for (a) methanol, (a) acetaldehyde, (c) ethanol, and (d) C_4-carbonyls including methacrolein (MACR), methyl vinyl ketone (MVK), and crotonaldehyde.

3.2.2. Interferences to m/z 45 from ethanol reactions with O_2^+

The most significant interference for the small oxygenated VOCs observed by GC-PTR-ToF-MS is associated with the ionization of ethanol to produce signal at the mass typically assigned to acetaldehyde (m/z 45, $C_2H_5O^+$). Ethanol has been shown by Inomata and Tanimoto (2009) to produce fragments at m/z 19 (H_3O^+), m/z 31 (CH_3O^+), and m/z 29 ($C_2H_5^+$). Buhr et al. (2002) identified m/z 45 as product and found that it correlated to the ethanol proton transfer product (m/z 47, $C_2H_6OH^+$) with a ratio of 0.22. The likely pathway for the formation of m/z 45 is by ethanol reactions with O_2^+, which has been identified by Spanel and Smith (1997) as the dominant O_2^+ product using selective ion flow tube (SIFT) mass spectrometry. The NOAA Vocus PTR-ToF-MS observes a ratio that is higher than that determined by Buhr et al. (2002) (~0.38), although the distribution of total fragmentation (i.e., the sum of all ethanol fragments relative to m/z 47) appears similar (Fig. S1).

Figure 11 shows the temporal behavior of m/z 45 and m/z 47 (ethanol) during the nighttime drive on 30 July. Figure 11a shows the mixing ratio of m/z 45 assuming the sensitivity of acetaldehyde and Fig. 11b shows the mixing ratio of ethanol. Figure 11c shows a scatter plot of the signal at m/z 45 vs. that of m/z 47 for the entire mobile laboratory dataset. First, ethanol and m/z 45 are correlated when ethanol mixing ratios are high (Fig. 11a, b). Ethanol on the Las Vegas Strip

reached mixing ratios of 1.5 ppm and corresponding increases in m/z 45 were observed that point towards a contribution from ethanol. Figure 11c shows that a subset of the m/z 45 signal measured throughout the Las Vegas dataset exhibit a ratio to ethanol that agrees with the fragmentation ratio observed from GC-PTR-ToF-MS measurements. These observations point towards a broader impact of ethanol on m/z 45 throughout the Las Vegas region.
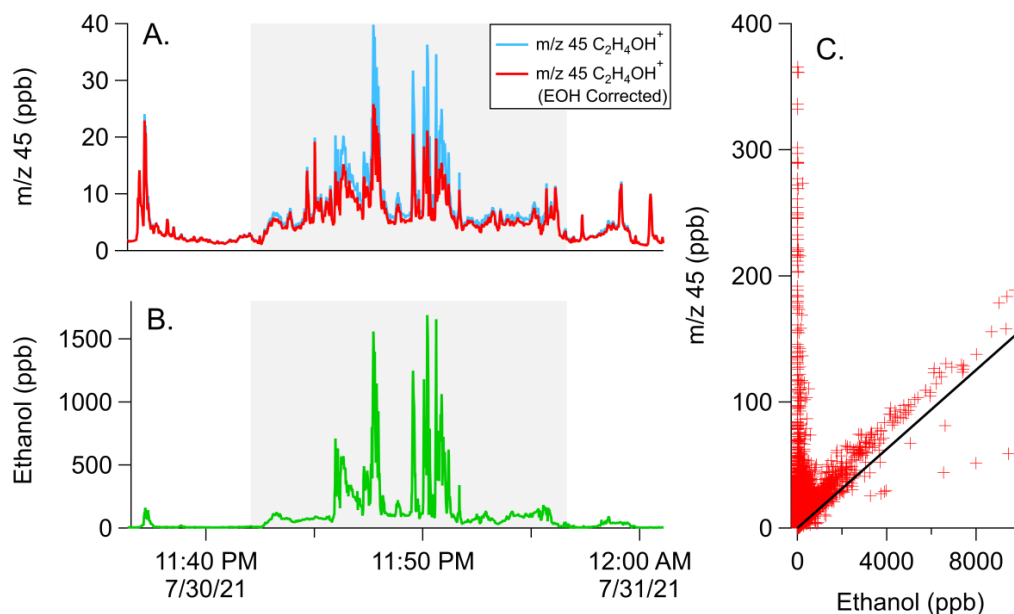
Figure 11. Demonstration of impacts of ethanol on mobile drive data in downtown Las Vegas during the evening drive on 30 July. (a) Time series of the signal at m/z 45 ($C_2H_4OH^+$) with and without the subtraction of the ethanol interference. (b) Time series of ethanol (m/z 47, $C_2H_6OH^+$). The shaded regions show when the mobile laboratory was sampling along the Las Vegas strip. (c) Correlation plot of mobile drive data for the entire Las Vegas dataset. The solid line shows the fragmentation ratio of m/z 45 to m/z 47 for ethanol, as derived from the GC-PTR-ToF-MS data (Fig. 10).

3.2.3. Corrections to m/z 45 measured in Las Vegas

The extent to which ethanol contributed to the signal at m/z 45 can be determined by correction techniques. Figure 11a shows the m/z 45 signal with the contribution from ethanol subtracted following:

$$\text{m/z 45}_{\text{Corrected}} = S_{45} - S_{47} \cdot f_{45/47} \quad \text{(Equation 2)}$$

S_{45} is the signal from m/z 45, S_{47} is the signal of ethanol, and $f_{45/47}$ is the ratio determined by GC-PTR-ToF-MS. Generally, the ethanol-corrected data on m/z 45 show that ethanol contributed ~40% to the signal on the Las Vegas Strip. Outside of this region, ethanol ionization has a modest impact on m/z 45. Over the average mobile laboratory dataset, ethanol may have contributed as much as 5% to the total signal at m/z 45. Similar contributions are estimated for the ground site data collected during ground sampling at Caltech. Consequently, ethanol reactions with O_2^+ may

932   only be an important contributor to m/z 45 in highly-concentrated ethanol plumes, which may be
933   encountered during mobile sampling or upon aircraft encounters with point sources. This ratio may
934   also be affected by humidity, which changes the distribution of O_2^+/H_3O^+ in drift tubes operated
935   at low water mixing ratio.
936
937   The GC-PTR-ToF-MS provides some insights into the interferences of oxygenates, but there are
938   limits to the extent to which oxygenates elute through a DB-624 or other GC columns with similar
939   polarity. Interferences towards oxygenated masses may be an important focus for future work, as
940   recent studies have pointed towards the increasing fraction of oxygenated VOCs observed in urban
941   air (Karl et al., 2018;Xu et al., 2022;Khare et al., 2022) and instrumentation capable of measuring
942   unfragmented oxygenates are becoming more common (e.g., Khare et al., 2022;Xu et al.,
943   2022;Riva et al., 2019). Intercomparisons with GC-MS measurements employing polar columns,
944   or with mass spectrometers employing softer ionization chemistry (e.g., iodide or NH_4^+ adduct
945   mass spectrometers) may help to better characterize the response and selectivity of PTR-ToF-MS
946   to oxygenates.
947
948   **3.3.   Aromatic VOCs**
949
950   **3.3.1. Known interferences to aromatic masses**
951
952   PTR-ToF-MS is well suited to measure ambient mixing ratios of C_6–C_9 aromatics; however, it is
953   known that alkyl aromatics (e.g., ethylbenzene and ethyltoluene isomers) and aromatic
954   monoterpenes and monoterpenoids (e.g., cymene and fenchone, Kari et al., 2018;Tani, 2013)
955   fragment and contribute to the signals typically attributed to benzene (m/z 79, $C_6H_6H^+$) and toluene
956   (m/z 93, $C_7H_8H^+$) (Pagonis et al., 2019;Yuan et al., 2017). The abundance and distribution of
957   aromatics depends on the relative mix of VOC emissions from petrochemical sources, including
958   fossil fuels, solvents emitted from VCPs (e.g. paints and architectural coatings), and asphalt paving
959   (Gkatzelis et al., 2021a;Gkatzelis et al., 2021b;Khare et al., 2020;Stockwell et al., 2021). Higher
960   aromatics, such as xylenes and ethylbenzene, are prevalent in both fossil fuel and VCP emissions,
961   whereas benzene is restricted in consumer products and is therefore almost entirely associated with
962   fossil fuels (McDonald et al., 2018). Consequently, PTR-ToF-MS measurements in urban regions
963   with significant solvent emissions may exhibit a greater degree of interference on benzene and
964   toluene than regions with greater fossil fuel usage.
965
966   **3.3.2. Characterizing interferences to benzene (m/z 79) using GC-PTR-ToF-MS**
967
968   Figure 12 shows GC-PTR-ToF-MS measurements of key aromatic compounds measured in
969   downtown Las Vegas where both fossil fuels and VCP emissions were prevalent. Each panel is
970   labeled by the typical compound assignment and shows chromatograms of the corresponding
971   proton-transfer product. In general, chromatograms show that C_9- and C_8-aromatics are the
972   expected key contributors to the signals at m/z 121 ($C_9H_{12}H^+$) and m/z 107 ($C_8H_{10}H^+$),
973   respectively. This is consistent with previously observed PTR-ToF-MS behavior (Yuan et al.,
974   2017), and shows that urban measurements at these masses continue to be reliably assigned to
975   simple alkyl aromatics.
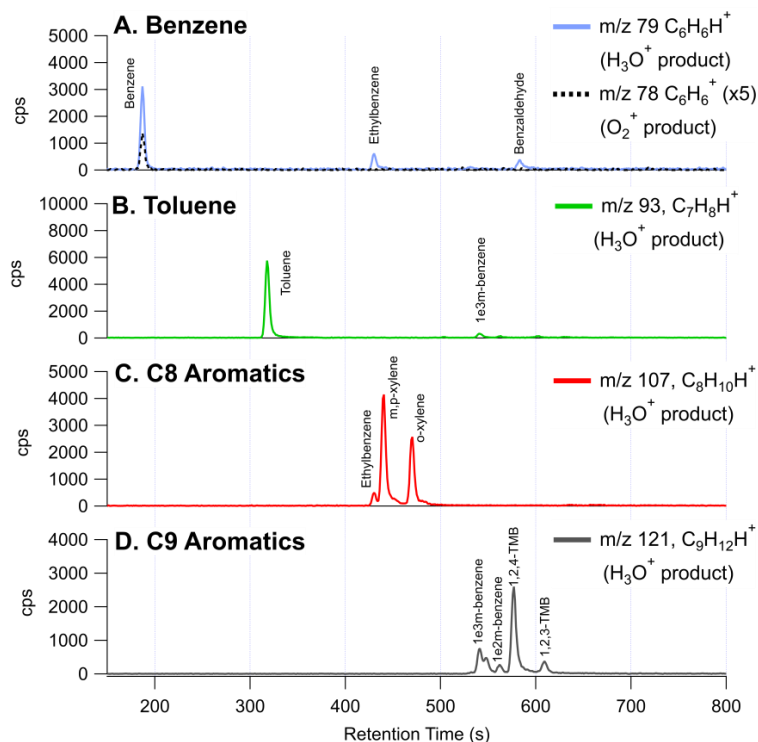
Figure 12. GC-PTR-ToF-MS chromatogram from downtown Las Vegas showing the contributions of isomers and fragments to ions typically assigned to C_6–C_9 aromatics. The labels highlight the traditionally assigned isomers for (a) benzene, (b) toluene, (c) C_8-aromatics including o,m,p-xylene + ethylbenzene, and (d) C_9-aromatics including ethyltoluene isomers + trimethylbenzene isomers.

In contrast, the masses typically assigned to benzene (m/z 79, $C_6H_6H^+$) and toluene (m/z 93, $C_7H_8H^+$) show greater contributions from the fragmentation of alkyl aromatics. At m/z 93, most of the signal is attributed to toluene and a small fraction ($< 5\%$) results from the fragmentation of 1-ethyl-3-methylbenzene. At m/z 79, ~ 80% of the signal results from the proton-transfer product of benzene and the remainder from the fragmentation of ethylbenzene and benzaldehyde. Previous work has shown contributions of ethylbenzene to m/z 79 in urban air (Inomata et al., 2010), whereas contributions from benzaldehyde are not well studied. Benzaldehyde may result from VCPs, cooking, motor vehicle emissions, biomass burning, or secondary production (Gkatzelis et al., 2021a;Koss et al., 2018;McDonald et al., 2018).

3.3.3. Corrections to ground site observations of m/z 79 in Los Angeles and Las Vegas

The interferences at m/z 79 are significant and present a challenge for reliably quantifying benzene in Las Vegas and other urban regions. To quantify this interference, Fig. 13 highlights benzene measurements from the Jerome Mack and Caltech ground sites. Figure 13a, b show corrected and uncorrected benzene at m/z 79 can be attributed to benzene calculated from two methods:

$$\text{m/z } 79_{\text{Corrected}} = S_{C6H6H+} - S_{C7H6OH+} \cdot f_{79/\text{Benzald}} - S_{C8H10H+} \cdot f_{79/\text{Ethylbenzene}} \quad \text{(Method 1)}$$

1000
1001
1002 $$m/z\ 79_{Corrected}\ =\ S_{C6H6+}\quad \text{(Method 2)}$$
1003
1004

1005 Where S_{C6H6H+} is the signal of $C_6H_6H^+$, $S_{C7H6OH+}$ is the signal attributable to benzaldehyde, $S_{C8H10H+}$
1006 is the signal attributable to ethylbenzene, and S_{C6H6+} is the signal attributed to the benzene charge-
1007 transfer product at m/z 78. $f_{79/Benzald}$ and $f_{79/Ethylbenzene}$ are the fragmentation patterns of
1008 benzaldehyde ($f_{79/Benzald} = C_6H_6H^+/C_7H_6OH^+$) and ethylbenzene ($f_{79/Ethylbenzene} = C_6H_6H^+/C_8H_{10}H^+$)
1009 as determined by GC-PTR-ToF-MS chromatograms. Method 1 corrects for benzene by subtracting
1010 the contributions of benzaldehyde and ethylbenzene to the signal at $C_6H_6H^+$. GC-PTR-ToF-MS
1011 measurements show that benzaldehyde is the primary contributor to $S_{C7H6OH+}$, whereas
1012 ethylbenzene is one of four isomers that contributes to $S_{C8H10H+}$. We use the GC-PTR-ToF-MS
1013 measurements at the Jerome Mack ground site and find that ethylbenzene contributes ~12.5% of
1014 the total C_8-aromatic signal. Method 2 simply estimates benzene mixing ratios based on
1015 calibrations applied to the charge-transfer product at m/z 78 ($C_6H_6^+$). This mass has no discernible
1016 interference from other VOCs in the GC-PTR-ToF-MS data (Fig. 12) and is detected with
1017 sufficient sensitivity to reliably quantify benzene (~180 cps ppb^{-1}). We note that Method 1 requires
1018 regular quantification of C_8-aromatic distributions by GC in order to account for ethylbenzene
1019 fragmentation, whereas Method 2 relies only on measurements of the O_2^+ charge-transfer product.
1020 We note that Method 2 may present limitations if other species are present that fragment to produce
1021 the O_2^+ product. Deployment of GC-PTR-ToF-MS in other cities may help to determine whether
1022 the charge-transfer product is unambiguously linked to benzene.
1023
1024 On average, the interferences from ethylbenzene and benzaldehyde constitute ~ 38% of the signal
1025 at m/z 79 detected at Jerome Mack, and ~ 3% of signal detected at Caltech (pie charts, Fig 13).
1026 We speciate the interference at Jerome Mack using GC-PTR-ToF-MS and find that the majority
1027 of the interference is associated with fragmentation of ethylbenzene (31% of total signal) with a
1028 small contribution from benzaldehyde (7% of total signal). Ethylbenzene was likely emitted from
1029 a local source due to a cabinet-making shop upwind of the ground site. The two methods for
1030 correcting benzene agree well for Jerome Mack data, which confirms that ethylbenzene and
1031 benzaldehyde are the primary contributors to the benzene interferences. We note that we only use
1032 Method 2 for data collected at Caltech since GC-PTR-ToF-MS measurements were unavailable
1033 during this period of the deployment.
1034
1035
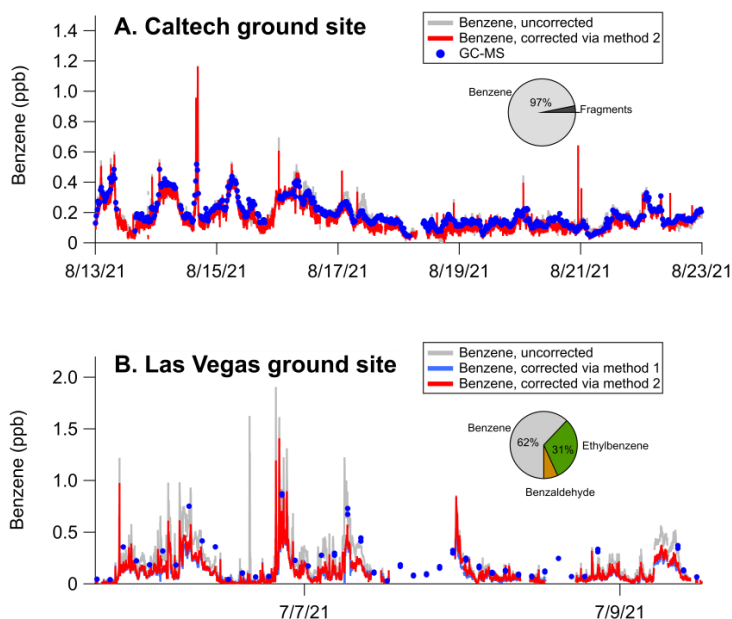
Figure 13. Impact of fragmentation on the signal at m/z 79 ($C_6H_6H^+$) and corresponding benzene mixing ratios measured at (a) Caltech and (b) the Jerome Mack ground site in Las Vegas. The corrections using the two methods are shown compared to uncorrected data. The pie charts show the average contribution of benzene, ethylbenzene, and benzaldehyde to the signal at m/z 79 ($C_6H_6H^+$).

3.3.4. Corrections to observations of m/z 79 in Detroit

The significant interferences to m/z 79 observed in Las Vegas are also observed in PTR-ToF-MS data collected downwind of Detroit during the MOOSE campaign. Figure 14 shows four days of mobile laboratory sampling with the Aerodyne PTR-ToF-MS and GC-MS instrumentation. Similar to Fig. 13, corrected via Method 2 and uncorrected m/z 79 measurements are shown (Fig. 14a). Figure 14b shows the histograms of PTR-ToF-MS measurements alongside those from the GC-MS during the entire campaign. The pie chart shows the average fraction of m/z 79 attributed to benzene vs. the fraction associated with fragments. Benzaldehyde and ethylbenzene contributions are not separated since GC-PTR-ToF-MS measurements were unavailable.
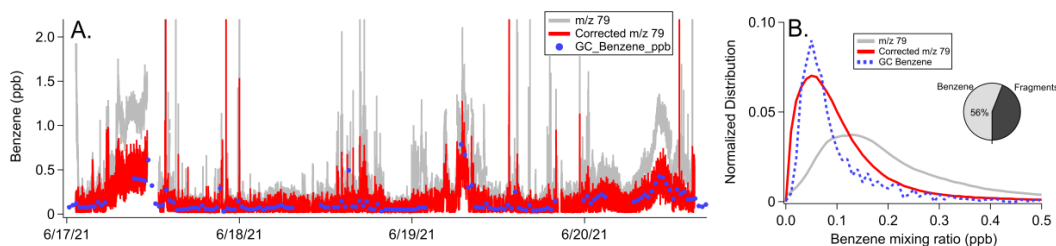
Figure 14. (a) Time series of GC-MS samples of benzene and PTR-ToF-MS mixing ratios of m/z 79 ($C_6H_6H^+$) and corrected m/z 79 reported during sampling by the Aerodyne Mobile Laboratory downwind of Detroit, MI. (b) Histograms showing the distribution of m/z 79 measured by the Aerodyne PTR-ToF-MS, corrected m/z 79 mixing ratios calculated using Method 2, and benzene mixing ratios measured by the GC-MS. The pie chart highlights the fraction of the m/z 79 associated with benzene vs. the fraction associated with fragments.

Similar to Las Vegas, fragmentation of higher aromatic species plays an important role in determining the benzene signal in m/z 79. The distribution of uncorrected m/z 79 shows a peak around 0.12 ppb and a broad tail biased towards higher mixing ratios. The GC-MS measures a distribution of benzene with a maximum at 0.05 ppb, and a much lower frequency of higher mixing ratios. When the PTR-ToF-MS data are calibrated using the benzene charge-transfer product (Method 2), corrected m/z 79 mixing ratios show a better agreement with GC-MS measurements. The distribution of corrected m/z 79 is wider than that reported by GC-MS, which may reflect the faster sampling of the PTR-ToF-MS and more frequent observations of concentrated aromatic plumes (Fig. 14a). Over the entire sampling period, the average distribution of m/z 79 shows that benzene accounts for ~ 56% of the total signal. This is consistent with the observations in Las Vegas (interference ~ 62% of the signal), indicating that m/z 79 in both datasets were influenced by solvent emissions to a significant extent.

4. Conclusions

Urban VOCs significantly contribute to the degradation of air quality, and PTR-ToF-MS provides important constraints on the emissions and chemical transformation of many gas-phase organics. Advances in PTR-ToF-MS sensitivity and detection provide opportunities to identify, characterize, and revisit measurement interferences to commonly reported VOCs (Yuan et al., 2017). Here, we find that long-chain aldehydes, along with previously identified cycloalkanes, are important contributors to the signal of m/z 69 typically associated with isoprene in many urban areas. The fragmentation of these molecules can be larger than the signal associated with the proton-transfer product from isoprene, depending on the mixture of anthropogenic and biogenic VOCs, time of day, and season. We find that interferences at ground level in Los Angeles (large isoprene emissions, large anthropogenic emissions) are highest at night and constitute ~10% of the signal observed during the day. Interferences are a higher fraction of m/z 69 at altitude (> 50%) and are observed to be widespread throughout the Los Angeles Basin. In Las Vegas (low isoprene emissions, large anthropogenic emissions), interferences dominate the signal at m/z 69 throughout the day and night. These interferences are observed in other cities (e.g., Detroit and New York City), depend on season, and are common among drift tube designs operated at similar E/N.

Other PTR-ToF-MS masses also exhibit interferences, including those typically assigned to oxygenates and aromatic VOCs. Fragmentation from ethanol impacts measurements of acetaldehyde on m/z 45, though this interference is only significant in regions with large ethanol emissions. PTR-ToF-MS measurements of benzene using m/z 79 exhibit significant interferences from the fragmentation of ethylbenzene and benzaldehyde. In Las Vegas and Detroit, fragmentation impacts m/z 79 mixing ratios by as much as 40%. The growing contribution of interferences to aromatics and oxygenates may reflect the changing mix of urban VOC emissions from one dominated by mobile sources to one dominated by solvents (Gkatzelis et al., 2021b;McDonald et al., 2018). In the case of benzene, other ions such as the charge-transfer product (m/z 78, $C_6H_6^+$) can be used to quantify benzene without significant influence from

1102 fragmentation from higher carbon VOCs. As instrument sensitivity improves, there may be other
1103 ions that can be used to improve the quantification of additional VOCs.

1105 Corrections to these interferences are feasible, though it is unlikely that a universal correction
1106 factor is sufficient to resolve instrument discrepancies across datasets. Instrument responses, as
1107 well as changes to the VOC mixture in different regions, require that detailed characterization be
1108 performed on a dataset-by-dataset basis. GC-MS measurements provide an opportunity to compare
1109 against PTR-ToF-MS measurements for a wide-variety of key VOCs, including isoprene, small
1110 oxygenates, and aromatics. Likewise, information about fragmentation and instrument-specific
1111 responses to reactive hydrocarbons can be determined using GC-PTR-ToF-MS. For species such
1112 as oxygenates, intercomparisons against other mass spectrometers using softer ionization (e.g.,
1113 iodide or ammonium-adduct CIMS) or use of GC pre-separation using polar columns may yield
1114 valuable information about instrument artifacts.

1116 **Data Availability**

1118 Data for SUNVEx and RE-CAP are available at the NOAA CSL data repository
1119 (https://csl.noaa.gov/projects/sunvex/). Data for FIREX-AQ, MOOSE, and LISTOS are available
1120 at the NASA data repository (https://www-air.larc.nasa.gov/missions.htm).

1122 **Author Contribution**

1124 MMC, CES, XL, JBG, AL, CW, EYP, CA, EFK, and AHG conducted measurements during
1125 SUNVEx and RE-CAP. MMC, GIG, CW, JBG, AL, AW, FP, DB, RH, and ECA conducted
1126 measurements during FIREX-AQ. MSC, BML, FM, and MC conducted measurements during
1127 MOOSE. JM, CC, and JEM conducted measurements during LISTOS. MMC and CW wrote the
1128 paper with contributions from all authors.

1130 **Competing Interests**

1132 EAC is a co-editor of Atmospheric Measurement Techniques. The peer-review process was guided
1133 by an independent editor and the authors also have no other competing interests to declare.

1135 **Acknowledgements**

References

Angevine, W. M., Brioude, J., McKeen, S., Holloway, J. S., Lerner, B. M., Goldstein, A. H., Guha, A., Andrews, A., Nowak, J. B., Evan, S., Fischer, M. L., Gilman, J. B., and Bon, D.: Pollutant transport among California regions, Journal of Geophysical Research: Atmospheres, 118, 6750-6763, https://doi.org/10.1002/jgrd.50490, 2013.

Annual Monitoring Network Plan, Clark County Department of Environment and Sustainability, 1-77, 2022.

Apel, E. C., Hornbrook, R. S., Hills, A. J., Blake, N. J., Barth, M. C., Weinheimer, A., Cantrell, C., Rutledge, S. A., Basarab, B., Crawford, J., Diskin, G., Homeyer, C. R., Campos, T., Flocke, F., Fried, A., Blake, D. R., Brune, W., Pollack, I., Peischl, J., Ryerson, T., Wennberg, P. O., Crounse, J. D., Wisthaler, A., Mikoviny, T., Huey, G., Heikes, B., O'Sullivan, D., and Riemer, D. D.: Upper tropospheric ozone production from lightning NOx-impacted convection: Smoke ingestion case study from the DC3 campaign, Journal of Geophysical Research: Atmospheres, 120, 2505-2523, https://doi.org/10.1002/2014JD022121, 2015.

Arata, C., Misztal, P. K., Tian, Y., Lunderberg, D. M., Kristensen, K., Novoselac, A., Vance, M. E., Farmer, D. K., Nazaroff, W. W., and Goldstein, A. H.: Volatile organic compound emissions during HOMEChem, Indoor Air, 31, 2099-2117, https://doi.org/10.1111/ina.12906, 2021.

Arnold, S. T., Viggiano, A. A., and Morris, R. A.: Rate Constants and Product Branching Fractions for the Reactions of H3O+ and NO+ with C2−C12 Alkanes, The Journal of Physical Chemistry A, 102, 8881-8887, 10.1021/jp9815457, 1998.

Breitenlechner, M., Fischer, L., Hainer, M., Heinritzi, M., Curtius, J., and Hansel, A.: PTR3: An Instrument for Studying the Lifecycle of Reactive Organic Carbon in the Atmosphere, Analytical Chemistry, 89, 5824-5831, 10.1021/acs.analchem.6b05110, 2017.

Buhr, K., van Ruth, S., and Delahunty, C.: Analysis of volatile flavour compounds by Proton Transfer Reaction-Mass Spectrometry: fragmentation patterns and discrimination between isobaric and isomeric compounds, International Journal of Mass Spectrometry, 221, 1-7, https://doi.org/10.1016/S1387-3806(02)00896-5, 2002.

Burkholder, J. B., Sander, S. P., Abbatt, J., Barker, J. R., Cappa, C., Crounse, J. D., Dibble, T. S., Huie, R. E., Kolb, C. E., Kurylo, M. J., Orkin, V. L., Percival, C. J., Wilmouth, D. M., and Wind, P. H.: Chemical Kinetics and Photochemical Data for Use in Atmospheric Studies, Evaluation No. 19, Jet Propulsion Laboratory, Pasadena, CA, 2019.

Calfapietra, C., Fares, S., Manes, F., Morani, A., Sgrigna, G., and Loreto, F.: Role of Biogenic Volatile Organic Compounds (BVOC) emitted by urban trees on ozone concentration in cities: A review, Environmental Pollution, 183, 71-80, https://doi.org/10.1016/j.envpol.2013.03.012, 2013.

1185   Cao, C., Gentner, D. R., Commane, R., Toledo-Crow, R., Schiferl, L. D., and Mak, J. E.: Policy-
1186   Related Gains in Urban Air Quality May Be Offset by Increased Emissions in a Warming Climate,
1187   Environmental Science & Technology, 10.1021/acs.est.2c05904, 2023.

1188   Choi, J., Henze, D. K., Cao, H., Nowlan, C. R., González Abad, G., Kwon, H.-A., Lee, H.-M., Oak, Y.
1189   J., Park, R. J., Bates, K. H., Maasakkers, J. D., Wisthaler, A., and Weinheimer, A. J.: An Inversion
1190   Framework for Optimizing Non-Methane VOC Emissions Using Remote Sensing and Airborne
1191   Observations in Northeast Asia During the KORUS-AQ Field Campaign, Journal of Geophysical
1192   Research: Atmospheres, 127, e2021JD035844, https://doi.org/10.1029/2021JD035844, 2022.

1193   Claflin, M. S., Pagonis, D., Finewax, Z., Handschy, A. V., Day, D. A., Brown, W. L., Jayne, J. T.,
1194   Worsnop, D. R., Jimenez, J. L., Ziemann, P. J., de Gouw, J., and Lerner, B. M.: An in situ gas
1195   chromatograph with automatic detector switching between PTR- and EI-TOF-MS: isomer-
1196   resolved measurements of indoor air, Atmos. Meas. Tech., 14, 133-152, 10.5194/amt-14-133-
1197   2021, 2021.

1198   Coggon, M. M., McDonald, B. C., Vlasenko, A., Veres, P. R., Bernard, F., Koss, A. R., Yuan, B.,
1199   Gilman, J. B., Peischl, J., Aikin, K. C., DuRant, J., Warneke, C., Li, S.-M., and de Gouw, J. A.:
1200   Diurnal Variability and Emission Pattern of Decamethylcyclopentasiloxane (D5) from the
1201   Application of Personal Care Products in Two North American Cities, Environmental Science &
1202   Technology, 52, 5610-5618, 10.1021/acs.est.8b00506, 2018.

1203   Coggon, M. M., Gkatzelis, G. I., McDonald, B. C., Gilman, J. B., Schwantes, R. H., Abuhassan, N.,
1204   Aikin, K. C., Arend, M. F., Berkoff, T. A., Brown, S. S., Campos, T. L., Dickerson, R. R., Gronoff, G.,
1205   Hurley, J. F., Isaacman-VanWertz, G., Koss, A. R., Li, M., McKeen, S. A., Moshary, F., Peischl, J.,
1206   Pospisilova, V., Ren, X., Wilson, A., Wu, Y., Trainer, M., and Warneke, C.: Volatile chemical
1207   product emissions enhance ozone and modulate urban chemistry, Proceedings of the National
1208   Academy of Sciences, 118, e2026653118, doi:10.1073/pnas.2026653118, 2021.

1209   Colman, J. J., Swanson, A. L., Meinardi, S., Sive, B. C., Blake, D. R., and Rowland, F. S.:
1210   Description of the Analysis of a Wide Range of Volatile Organic Compounds in Whole Air
1211   Samples Collected during PEM-Tropics A and B, Analytical Chemistry, 73, 3723-3731,
1212   10.1021/ac010027g, 2001.

1213   Ernle, L., Ringsdorf, M. A., and Williams, J.: Influence of ozone and humidity on PTR-MS and GC-
1214   MS VOC measurements with and without a Na2S2O3 ozone scrubber, Atmos. Meas. Tech., 16,
1215   1179-1194, 10.5194/amt-16-1179-2023, 2023.

1216   Gkatzelis, G. I., Coggon, M. M., McDonald, B. C., Peischl, J., Aikin, K. C., Gilman, J. B., Trainer, M.,
1217   and Warneke, C.: Identifying Volatile Chemical Product Tracer Compounds in U.S. Cities,
1218   Environmental Science & Technology, 55, 188-199, 10.1021/acs.est.0c05467, 2021a.

1219   Gkatzelis, G. I., Coggon, M. M., McDonald, B. C., Peischl, J., Gilman, J. B., Aikin, K. C., Robinson,
1220   M. A., Canonaco, F., Prevot, A. S. H., Trainer, M., and Warneke, C.: Observations Confirm that

Volatile Chemical Products Are a Major Source of Petrochemical Emissions in U.S. Cities, Environmental Science & Technology, 55, 4332-4343, 10.1021/acs.est.0c05471, 2021b.

Gkatzelis, G. I., Coggon, M. M., Stockwell, C. E., Hornbrook, R. S., Allen, H., Apel, E. C., Bela, M. M., Blake, D. R., Bourgeois, I., Brown, S. S., Campuzano-Jost, P., St. Clair, J. M., Crawford, J. H., Crounse, J., Day, D. A., DiGangi, J. P., Diskin, G. S., Fried, A., Gilman, J. B., Guo, H., Hair, J. W., Halliday, H. S., Hanisco, T. F., Hannun, R. A., Hills, A., Huey, L. G., Jimenez, J. L., Katich, J. M., Lamplugh, A., Lee, Y. R., Liao, J., Neuman, J. A., Nowak, J. B., Pagonis, D., Peischl, J., Perring, A. E., Piel, F., Rickly, P. S., Robinson, M. A., Rollins, A. W., Ryerson, T. B., Schueneman, M. K., Schwantes, R. H., Schwarz, J. P., Sekimoto, K., Selimovic, V., Shingler, T., Tanner, D. J., Tomsche, L., Vasquez, K. T., Veres, P., Washenfelder, R. A., Weibring, P., Wennberg, P. O., Wisthaler, A., Wolfe, G. M., Womack, C. C., Xu, L., Yokelson, R., and Warneke, C.: Parameterizations of US wildfire and prescribed fire emission ratios and emission factors based on FIREX-AQ aircraft measurements, Atmos. Chem. Phys., In prep, 2022.

Gueneron, M., Erickson, M. H., VanderSchelden, G. S., and Jobson, B. T.: PTR-MS fragmentation patterns of gasoline hydrocarbons, International Journal of Mass Spectrometry, 379, 97-109, https://doi.org/10.1016/j.ijms.2015.01.001, 2015.

Guenther, A. B., Jiang, X., Heald, C. L., Sakulyanontvittaya, T., Duhl, T., Emmons, L. K., and Wang, X.: The Model of Emissions of Gases and Aerosols from Nature version 2.1 (MEGAN2.1): an extended and updated framework for modeling biogenic emissions, Geosci. Model Dev., 5, 1471-1492, 10.5194/gmd-5-1471-2012, 2012.

Herndon, S. C., Jayne, J. T., Zahniser, M. S., Worsnop, D. R., Knighton, B., Alwine, E., Lamb, B. K., Zavala, M., Nelson, D. D., McManus, J. B., Shorter, J. H., Canagaratna, M. R., Onasch, T. B., and Kolb, C. E.: Characterization of urban pollutant emission fluxes and ambient concentration distributions using a mobile laboratory with rapid response instrumentation, Faraday Discussions, 130, 327-339, 10.1039/B500411J, 2005.

Holzinger, R., Acton, W. J. F., Bloss, W. J., Breitenlechner, M., Crilley, L. R., Dusanter, S., Gonin, M., Gros, V., Keutsch, F. N., Kiendler-Scharr, A., Kramer, L. J., Krechmer, J. E., Languille, B., Locoge, N., Lopez-Hilfiker, F., Materić, D., Moreno, S., Nemitz, E., Quéléver, L. L. J., Sarda Esteve, R., Sauvage, S., Schallhart, S., Sommariva, R., Tillmann, R., Wedel, S., Worton, D. R., Xu, K., and Zaytsev, A.: Validity and limitations of simple reaction kinetics to calculate concentrations of organic compounds from ion counts in PTR-MS, Atmos. Meas. Tech., 12, 6193-6208, 10.5194/amt-12-6193-2019, 2019.

Inomata, S., and Tanimoto, H.: A deuterium-labeling study on the reproduction of hydronium ions in the PTR-MS detection of ethanol, International Journal of Mass Spectrometry, 285, 95-99, https://doi.org/10.1016/j.ijms.2009.05.001, 2009.

Inomata, S., Tanimoto, H., Kato, S., Suthawaree, J., Kanaya, Y., Pochanart, P., Liu, Y., and Wang, Z.: PTR-MS measurements of non-methane volatile organic compounds during an intensive field

1258   campaign at the summit of Mount Tai, China, in June 2006, Atmos. Chem. Phys., 10, 7085-7099,
1259   10.5194/acp-10-7085-2010, 2010.

1260   Jobson, B. T., Alexander, M. L., Maupin, G. D., and Muntean, G. G.: On-line analysis of organic
1261   compounds in diesel exhaust using a proton transfer reaction mass spectrometer (PTR-MS),
1262   International Journal of Mass Spectrometry, 245, 78-89,
1263   https://doi.org/10.1016/j.ijms.2005.05.009, 2005.

1264   Kari, E., Miettinen, P., Yli-Pirilä, P., Virtanen, A., and Faiola, C. L.: PTR-ToF-MS product ion
1265   distributions and humidity-dependence of biogenic volatile organic compounds, International
1266   Journal of Mass Spectrometry, 430, 87-97, https://doi.org/10.1016/j.ijms.2018.05.003, 2018.

1267   Karl, T., Hansel, A., Cappellin, L., Kaser, L., Herdlinger-Blatt, I., and Jud, W.: Selective
1268   measurements of isoprene and 2-methyl-3-buten-2-ol based on NO^+ ionization
1269   mass spectrometry, Atmos. Chem. Phys., 12, 11877-11884, 10.5194/acp-12-11877-2012, 2012.

1270   Karl, T., Striednig, M., Graus, M., Hammerle, A., and Wohlfahrt, G.: Urban flux measurements
1271   reveal a large pool of oxygenated volatile organic compound emissions, Proc. Natl. Acad. Sci.
1272   U.S.A., 115, 1186-1191, 10.1073/pnas.1714715115, 2018.

1273   Kaser, L., Karl, T., Schnitzhofer, R., Graus, M., Herdlinger-Blatt, I. S., DiGangi, J. P., Sive, B.,
1274   Turnipseed, A., Hornbrook, R. S., Zheng, W., Flocke, F. M., Guenther, A., Keutsch, F. N., Apel, E.,
1275   and Hansel, A.: Comparison of different real time VOC measurement techniques in a ponderosa
1276   pine forest, Atmos. Chem. Phys., 13, 2893-2906, 10.5194/acp-13-2893-2013, 2013.

1277   Khare, P., Machesky, J., Soto, R., He, M., Presto, A. A., and Gentner, D. R.: Asphalt-related
1278   emissions are a major missing nontraditional source of secondary organic aerosol precursors,
1279   Science Advances, 6, eabb9785, doi:10.1126/sciadv.abb9785, 2020.

1280   Khare, P., Krechmer, J. E., Machesky, J. E., Hass-Mitchell, T., Cao, C., Wang, J., Majluf, F., Lopez-
1281   Hilfiker, F., Malek, S., Wang, W., Seltzer, K., Pye, H. O. T., Commane, R., McDonald, B. C.,
1282   Toledo-Crow, R., Mak, J. E., and Gentner, D. R.: Ammonium adduct chemical ionization to
1283   investigate anthropogenic oxygenated gas-phase organic compounds in urban air, Atmos.
1284   Chem. Phys., 22, 14377-14399, 10.5194/acp-22-14377-2022, 2022.

1285   Kilgour, D., Novak, G., and Bertram, T.: Observations of Biotic and Abiotic Marine Volatile
1286   Organic Compounds Emitted from Coastal Seawater, December 01, 2021, 2021.

1287   Kim, S.-W., McDonald, B. C., Seo, S., Kim, K.-M., and Trainer, M.: Understanding the Paths of
1288   Surface Ozone Abatement in the Los Angeles Basin, Journal of Geophysical Research:
1289   Atmospheres, 127, e2021JD035606, https://doi.org/10.1029/2021JD035606, 2022.

1290   Klein, F., Platt, S. M., Farren, N. J., Detournay, A., Bruns, E. A., Bozzetti, C., Daellenbach, K. R.,
1291   Kilic, D., Kumar, N. K., Pieber, S. M., Slowik, J. G., Temime-Roussel, B., Marchand, N., Hamilton,
1292   J. F., Baltensperger, U., Prévôt, A. S. H., and El Haddad, I.: Characterization of Gas-Phase

1293   Organics Using Proton Transfer Reaction Time-of-Flight Mass Spectrometry: Cooking Emissions,
1294   Environmental Science & Technology, 50, 1243-1250, 10.1021/acs.est.5b04618, 2016.

1295   Koss, A., Yuan, B., Warneke, C., Gilman, J. B., Lerner, B. M., Veres, P. R., Peischl, J., Eilerman, S.,
1296   Wild, R., Brown, S. S., Thompson, C. R., Ryerson, T., Hanisco, T., Wolfe, G. M., Clair, J. M. S.,
1297   Thayer, M., Keutsch, F. N., Murphy, S., and de Gouw, J.: Observations of VOC emissions and
1298   photochemical products over US oil- and gas-producing regions using high-resolution H3O+
1299   CIMS (PTR-ToF-MS), Atmos. Meas. Tech., 10, 2941-2968, 10.5194/amt-10-2941-2017, 2017.

1300   Koss, A. R., Sekimoto, K., Gilman, J. B., Selimovic, V., Coggon, M. M., Zarzana, K. J., Yuan, B.,
1301   Lerner, B. M., Brown, S. S., Jimenez, J. L., Krechmer, J., Roberts, J. M., Warneke, C., Yokelson, R.
1302   J., and de Gouw, J.: Non-methane organic gas emissions from biomass burning: identification,
1303   quantification, and emission factors from PTR-ToF during the FIREX 2016 laboratory
1304   experiment, Atmos. Chem. Phys., 18, 3299-3319, 10.5194/acp-18-3299-2018, 2018.

1305   Krechmer, J., Lopez-Hilfiker, F., Koss, A., Hutterli, M., Stoermer, C., Deming, B., Kimmel, J.,
1306   Warneke, C., Holzinger, R., Jayne, J., Worsnop, D., Fuhrer, K., Gonin, M., and de Gouw, J.:
1307   Evaluation of a New Reagent-Ion Source and Focusing Ion–Molecule Reactor for Use in Proton-
1308   Transfer-Reaction Mass Spectrometry, Analytical Chemistry, 90, 12011-12018,
1309   10.1021/acs.analchem.8b02641, 2018.

1310   Lerner, B. M., Gilman, J. B., Aikin, K. C., Atlas, E. L., Goldan, P. D., Graus, M., Hendershot, R.,
1311   Isaacman-VanWertz, G. A., Koss, A., Kuster, W. C., Lueb, R. A., McLaughlin, R. J., Peischl, J.,
1312   Sueper, D., Ryerson, T. B., Tokarek, T. W., Warneke, C., Yuan, B., and de Gouw, J. A.: An
1313   improved, automated whole air sampler and gas chromatography mass spectrometry analysis
1314   system for volatile organic compounds in the atmosphere, Atmos. Meas. Tech., 10, 291-313,
1315   10.5194/amt-10-291-2017, 2017.

1316   McDonald, B. C., de Gouw, J. A., Gilman, J. B., Jathar, S. H., Akherati, A., Cappa, C. D., Jimenez, J.
1317   L., Lee-Taylor, J., Hayes, P. L., McKeen, S. A., Cui, Y. Y., Kim, S. W., Gentner, D. R., Isaacman-
1318   VanWertz, G., Goldstein, A. H., Harley, R. A., Frost, G. J., Roberts, J. M., Ryerson, T. B., and
1319   Trainer, M.: Volatile chemical products emerging as largest petrochemical source of urban
1320   organic emissions, Science, 359, 760-764, 10.1126/science.aaq0524, 2018.

1321   Müller, M., Mikoviny, T., Feil, S., Haidacher, S., Hanel, G., Hartungen, E., Jordan, A., Märk, L.,
1322   Mutschlechner, P., Schottkowsky, R., Sulzer, P., Crawford, J. H., and Wisthaler, A.: A compact
1323   PTR-ToF-MS instrument for airborne measurements of volatile organic compounds at high
1324   spatiotemporal resolution, Atmos. Meas. Tech., 7, 3763-3772, 10.5194/amt-7-3763-2014, 2014.

1325   Pagonis, D., Sekimoto, K., and de Gouw, J.: A Library of Proton-Transfer Reactions of H3O+ Ions
1326   Used for Trace Gas Detection, Journal of The American Society for Mass Spectrometry, 30,
1327   1330-1335, 10.1007/s13361-019-02209-3, 2019.

1328   Peng, Y., Mouat, A. P., Hu, Y., Li, M., McDonald, B. C., and Kaiser, J.: Source appointment of
1329   volatile organic compounds and evaluation of anthropogenic monoterpene emission estimates

1330   in Atlanta, Georgia, Atmospheric Environment, 288, 119324,
1331   https://doi.org/10.1016/j.atmosenv.2022.119324, 2022.

1332   Pfannerstill, E. Y., Wang, N., Edtbauer, A., Bourtsoukidis, E., Crowley, J. N., Dienhart, D., Eger, P.
1333   G., Ernle, L., Fischer, H., Hottmann, B., Paris, J. D., Stönner, C., Tadic, I., Walter, D., Lelieveld, J.,
1334   and Williams, J.: Shipborne measurements of total OH reactivity around the Arabian Peninsula
1335   and its role in ozone chemistry, Atmos. Chem. Phys., 19, 11501-11523, 10.5194/acp-19-11501-
1336   2019, 2019.

1337   Pfannerstill, E. Y., Arata, C., Zhu, Q., Schulze, B. C., Woods, R., Seinfeld, J. H., Bucholtz, A.,
1338   Cohen, R. C., and Goldstein, A. H.: Volatile organic compound fluxes in the San Joaquin Valley –
1339   spatial distribution, source attribution, and inventory comparison, EGUsphere, 2023, 1-42,
1340   10.5194/egusphere-2023-723, 2023.

1341   Riva, M., Rantala, P., Krechmer, J. E., Peräkylä, O., Zhang, Y., Heikkinen, L., Garmash, O., Yan, C.,
1342   Kulmala, M., Worsnop, D., and Ehn, M.: Evaluating the performance of five different chemical
1343   ionization techniques for detecting gaseous oxygenated organic species, Atmos. Meas. Tech.,
1344   12, 2403-2421, 10.5194/amt-12-2403-2019, 2019.

1345   Rivera-Rios, J. C., Nguyen, T. B., Crounse, J. D., Jud, W., St. Clair, J. M., Mikoviny, T., Gilman, J. B.,
1346   Lerner, B. M., Kaiser, J. B., de Gouw, J., Wisthaler, A., Hansel, A., Wennberg, P. O., Seinfeld, J. H.,
1347   and Keutsch, F. N.: Conversion of hydroperoxides to carbonyls in field and laboratory
1348   instrumentation: Observational bias in diagnosing pristine versus anthropogenically controlled
1349   atmospheric chemistry, Geophysical Research Letters, 41, 8645-8651,
1350   https://doi.org/10.1002/2014GL061919, 2014.

1351   Romano, A., and Hanna, G. B.: Identification and quantification of VOCs by proton transfer
1352   reaction time of flight mass spectrometry: An experimental workflow for the optimization of
1353   specificity, sensitivity, and accuracy, Journal of Mass Spectrometry, 53, 287-295,
1354   https://doi.org/10.1002/jms.4063, 2018.

1355   Ryerson, T. B., Andrews, A. E., Angevine, W. M., Bates, T. S., Brock, C. A., Cairns, B., Cohen, R. C.,
1356   Cooper, O. R., de Gouw, J. A., Fehsenfeld, F. C., Ferrare, R. A., Fischer, M. L., Flagan, R. C.,
1357   Goldstein, A. H., Hair, J. W., Hardesty, R. M., Hostetler, C. A., Jimenez, J. L., Langford, A. O.,
1358   McCauley, E., McKeen, S. A., Molina, L. T., Nenes, A., Oltmans, S. J., Parrish, D. D., Pederson, J.
1359   R., Pierce, R. B., Prather, K., Quinn, P. K., Seinfeld, J. H., Senff, C. J., Sorooshian, A., Stutz, J.,
1360   Surratt, J. D., Trainer, M., Volkamer, R., Williams, E. J., and Wofsy, S. C.: The 2010 California
1361   Research at the Nexus of Air Quality and Climate Change (CalNex) field study, Journal of
1362   Geophysical Research: Atmospheres, 118, 5830-5866, https://doi.org/10.1002/jgrd.50331,
1363   2013.

1364   Schauer, J. J., Kleeman, M. J., Cass, G. R., and Simoneit, B. R. T.: Measurement of Emissions from
1365   Air Pollution Sources. 1. C1 through C29 Organic Compounds from Meat Charbroiling,
1366   Environmental Science & Technology, 33, 1566-1577, 10.1021/es980076j, 1999.

1367 Sekimoto, K., Li, S.-M., Yuan, B., Koss, A., Coggon, M., Warneke, C., and de Gouw, J.: Calculation
1368 of the sensitivity of proton-transfer-reaction mass spectrometry (PTR-MS) for organic trace
1369 gases using molecular properties, International Journal of Mass Spectrometry, 421, 71-94,
1370 https://doi.org/10.1016/j.ijms.2017.04.006, 2017.

1371 Simpson, I. J., Blake, N. J., Barletta, B., Diskin, G. S., Fuelberg, H. E., Gorham, K., Huey, L. G.,
1372 Meinardi, S., Rowland, F. S., Vay, S. A., Weinheimer, A. J., Yang, M., and Blake, D. R.:
1373 Characterization of trace gases measured over Alberta oil sands mining operations: 76
1374 speciated C_2–C_{10} volatile organic compounds (VOCs),
1375 CO_2, CH_4, CO, NO, NO_2, NO_y,
1376 O_3 and SO_2, Atmos. Chem. Phys., 10, 11931-11954, 10.5194/acp-10-
1377 11931-2010, 2010.

1378 Simpson, I. J., Blake, D. R., Blake, N. J., Meinardi, S., Barletta, B., Hughes, S. C., Fleming, L. T.,
1379 Crawford, J. H., Diskin, G. S., Emmons, L. K., Fried, A., Guo, H., Peterson, D. A., Wisthaler, A.,
1380 Woo, J.-H., Barré, J., Gaubert, B., Kim, J., Kim, M. J., Kim, Y., Knote, C., Mikoviny, T., Pusede, S.
1381 E., Schroeder, J. R., Wang, Y., Wennberg, P. O., and Zeng, L.: Characterization, sources and
1382 reactivity of volatile organic compounds (VOCs) in Seoul and surrounding regions during
1383 KORUS-AQ, Elementa: Science of the Anthropocene, 8, 10.1525/elementa.434, 2020.

1384 Spanel, P., and Smith, D.: SIFT studies of the reactions of H3O+, NO+ and O2+ with a series of
1385 alcohols, International Journal of Mass Spectrometry and Ion Processes, 167-168, 375-388,
1386 https://doi.org/10.1016/S0168-1176(97)00085-2, 1997.

1387 Stark, H., Yatavelli, R. L. N., Thompson, S. L., Kimmel, J. R., Cubison, M. J., Chhabra, P. S.,
1388 Canagaratna, M. R., Jayne, J. T., Worsnop, D. R., and Jimenez, J. L.: Methods to extract
1389 molecular and bulk chemical information from series of complex mass spectra with limited
1390 mass resolution, International Journal of Mass Spectrometry, 389, 26-38,
1391 https://doi.org/10.1016/j.ijms.2015.08.011, 2015.

1392 Stockwell, C. E., Coggon, M. M., Gkatzelis, G. I., Ortega, J., McDonald, B. C., Peischl, J., Aikin, K.,
1393 Gilman, J. B., Trainer, M., and Warneke, C.: Volatile organic compound emissions from solvent-
1394 and water-borne coatings – compositional differences and tracer compound identifications,
1395 Atmos. Chem. Phys., 21, 6005-6022, 10.5194/acp-21-6005-2021, 2021.

1396 Tani, A.: Fragmentation and Reaction Rate Constants of Terpenoids Determined by Proton
1397 Transfer Reaction-mass Spectrometry, Environmental Control in Biology, 51, 23-29,
1398 10.2525/ecb.51.23, 2013.

1399 Tomsche, L., Piel, F., Mikoviny, T., Nielsen, C. J., Guo, H., Campuzano-Jost, P., Nault, B. A.,
1400 Schueneman, M. K., Jimenez, J. L., Halliday, H., Diskin, G., DiGangi, J. P., Nowak, J. B., Wiggins, E.
1401 B., Gargulinski, E., Soja, A. J., and Wisthaler, A.: Measurement report: Emission factors of NH3
1402 and NHx for wildfires and agricultural fires in the United States, Atmos. Chem. Phys., 23, 2331-
1403 2343, 10.5194/acp-23-2331-2023, 2023.

1404   Vermeuel, M. P., Novak, G. A., Kilgour, D. B., Claflin, M. S., Lerner, B. M., Trowbridge, A. M.,
1405   Thom, J., Cleary, P. A., Desai, A. R., and Bertram, T. H.: Observations of biogenic volatile organic
1406   compounds over a mixed temperate forest during the summer to autumn transition,
1407   EGUsphere, 2022, 1-44, 10.5194/egusphere-2022-1015, 2022.

1408   Warneke, C., de Gouw, J. A., Kuster, W. C., Goldan, P. D., and Fall, R.: Validation of Atmospheric
1409   VOC Measurements by Proton-Transfer- Reaction Mass Spectrometry Using a Gas-
1410   Chromatographic Preseparation Method, Environmental Science & Technology, 37, 2494-2501,
1411   10.1021/es026266i, 2003.

1412   Warneke, C., de Gouw, J. A., Holloway, J. S., Peischl, J., Ryerson, T. B., Atlas, E., Blake, D.,
1413   Trainer, M., and Parrish, D. D.: Multiyear trends in volatile organic compounds in Los Angeles,
1414   California: Five decades of decreasing emissions, J. Geophs. Res., 117, 1-10,
1415   10.1029/2012jd017899, 2012.

1416   Warneke, C., Geiger, F., Edwards, P. M., Dube, W., Pétron, G., Kofler, J., Zahn, A., Brown, S. S.,
1417   Graus, M., Gilman, J. B., Lerner, B. M., Peischl, J., Ryerson, T. B., de Gouw, J. A., and Roberts, J.
1418   M.: Volatile organic compound emissions from the oil and natural gas industry in the Uintah
1419   Basin, Utah: oil and gas well pad emissions compared to ambient air composition, Atmos.
1420   Chem. Phys., 14, 10977-10988, 10.5194/acp-14-10977-2014, 2014.

1421   Warneke, C., Schwarz, J. P., Dibb, J., Kalashnikova, O., Frost, G., Al-Saad, J., Brown, S. S., Brewer,
1422   W. A., Soja, A., Seidel, F. C., Washenfelder, R. A., Wiggins, E. B., Moore, R. H., Anderson, B. E.,
1423   Jordan, C., Yacovitch, T. I., Herndon, S. C., Liu, S., Kuwayama, T., Jaffe, D., Johnston, N.,
1424   Selimovic, V., Yokelson, R., Giles, D. M., Holben, B. N., Goloub, P., Popovici, I., Trainer, M.,
1425   Kumar, A., Pierce, R. B., Fahey, D., Roberts, J., Gargulinski, E. M., Peterson, D. A., Ye, X., Thapa,
1426   L. H., Saide, P. E., Fite, C. H., Holmes, C. D., Wang, S., Coggon, M. M., Decker, Z. C. J., Stockwell,
1427   C. E., Xu, L., Gkatzelis, G., Aikin, K., Lefer, B., Kaspari, J., Griffin, D., Zeng, L., Weber, R., Hastings,
1428   M., Chai, J., Wolfe, G. M., Hanisco, T. F., Liao, J., Campuzano Jost, P., Guo, H., Jimenez, J. L.,
1429   Crawford, J., and Team, T. F.-A. S.: Fire Influence on Regional to Global Environments and Air
1430   Quality (FIREX-AQ), Journal of Geophysical Research: Atmospheres, 128, e2022JD037758,
1431   https://doi.org/10.1029/2022JD037758, 2023.

1432   Wernis, R. A., Kreisberg, N. M., Weber, R. J., Drozd, G. T., and Goldstein, A. H.: Source
1433   apportionment of VOCs, IVOCs and SVOCs by positive matrix factorization in suburban
1434   Livermore, California, Atmos. Chem. Phys., 22, 14987-15019, 10.5194/acp-22-14987-2022,
1435   2022.

1436   Xu, L., Coggon, M. M., Stockwell, C. E., Gilman, J. B., Robinson, M. A., Breitenlechner, M.,
1437   Lamplugh, A., Crounse, J. D., Wennberg, P. O., Neuman, J. A., Novak, G. A., Veres, P. R., Brown,
1438   S. S., and Warneke, C.: Chemical ionization mass spectrometry utilizing ammonium ions (NH_4^+
1439   CIMS) for measurements of organic compounds in the atmosphere, Atmos. Meas. Tech., 15,
1440   7353-7373, 10.5194/amt-15-7353-2022, 2022.

1441   Yacovitch, T. I., Herndon, S. C., Pétron, G., Kofler, J., Lyon, D., Zahniser, M. S., and Kolb, C. E.:
1442   Mobile Laboratory Observations of Methane Emissions in the Barnett Shale Region,
1443   Environmental Science & Technology, 49, 7889-7895, 10.1021/es506352j, 2015.

1444   Yuan, B., Koss, A., Warneke, C., Gilman, J. B., Lerner, B. M., Stark, H., and de Gouw, J. A.: A high-
1445   resolution time-of-flight chemical ionization mass spectrometer utilizing hydronium ions (H3O+
1446   ToF-CIMS) for measurements of volatile organic compounds in the atmosphere, Atmos. Meas.
1447   Tech., 9, 2735-2752, 10.5194/amt-9-2735-2016, 2016.

1448   Yuan, B., Koss, A. R., Warneke, C., Coggon, M., Sekimoto, K., and de Gouw, J. A.: Proton-
1449   Transfer-Reaction Mass Spectrometry: Applications in Atmospheric Sciences, Chem. Rev., 117,
1450   13187-13229, 10.1021/acs.chemrev.7b00325, 2017.
1451